Design, Development, and Experimentation of Stress and Strain Measurement System for Vertical Axis Wind Turbine (VAWT) blades

By

Deepak Sapkota

2262144

Thesis
Submitted to Flinders University
for the degree of

Master of Engineering (Mechanical)

College of Science and Engineering
05/12/2023

CONTENTS

ABSTRACT

The project is affiliated with the identification and development of a stress and strain measurement system for the Vertical Axis Wind Turbine (VAWT) blades carried out under the collaboration of the VAWT-X Energy and Flinders University. The project aims to identify the appropriate stress & strain measurement system suitable for rotatory VAWT blades capable to fit within the compact space of the VAWT blade geometry and measure different forms of stresses and strains with wire/wireless data transmission. To achieve these objectives, necessary literature reviews about different existing measurement systems, data acquisition systems, data analysis, and interpretation methods were studied. The project is based on the use of strain gages using quarter bridge configurations along-with affordable electronics components like Analog-digital converters (ADC), multiplexers for multiple sensor configurations, and a microcontroller with ESP 32 as part of the data acquisition system using Arduino programming for the data collection. The mathematical and theoretical approach is used for the conversion, analysis, and interpretation of the data obtained from the testing of the test model made of an assembly of 3 hollow VAWT blades capable of fitting the designed measurement system. The digital output data from the measurement system is interpreted to the values of principal stresses and strains by the intermediate conversion into differential voltage generated in the quarter bridge circuit. The obtained values are then validated with the FEA analysis of the test model in ANSYS. The proposed test model was experimented with static structural analysis having multiple loadings at each end with the arrangement of fixed support. The measurement system attached is suitable for the VAWT blades facilitating the use of blades' hollow cavity for the installation of components and transmission of data throughout the system. The measurement system is found to be sensitive to minor loadings tested under 5 different loading conditions and provided repeatable and quantifiable results. The experimental results and FEA results of the test specimen under static structural analysis are found to be satisfactorily close to each other.

Key Words; VAWT-X Energy, Strain gages, Quarter bridge circuit, Analog to Digital Convertor, ESP-32, Arduino programming

DECLARATION

I certify that this thesis:

3.1 does not incorporate without acknowledgment any material previously submitted for a degree or diploma in any university

3.2 and the research within will not be submitted for any other future degree or diploma without the permission of Flinders University; and

3.3 to the best of my knowledge and belief, does not contain any material previously published or written by another person except where due reference is made in the text.

Signature of student…..

Print name of student.....DEEPAK SAPKOTA.....

Date.....30/11/2023.....

I certify that I have read this thesis. In my opinion, it is/is not (please circle) fully adequate, in scope and quality, as a thesis for the degree of Master of Mechanical Engineering. Furthermore, I confirm that I have provided feedback on this thesis and the student has implemented it minimally/partially/fully (please circle).

Signature of Principal Supervisor…. .....

Print name of Principal Supervisor.....AMIR ZANJ.....

Date..30/11/2023.....

ACKNOWLEDGEMENTS

I would like to express my sincere gratitude to my supervisor Dr. Amir Zanj for his continuous guidance and support in every step during the project execution. His extraordinary expertise and constructive feedback at every stage have been crucial for the accomplishment of this Thesis project.

I would like to thank Mr. Gary Andrews, the C.E.O of VAWT-X Energy for providing me the opportunity to work on such an interesting innovative project that would be able to bring a positive impact on the R&D of the company.

I would like to express my deepest appreciation to Mr. Craig Dawson from the Flinders Engineering Services team who has guided me in every stage of the project development. His experience and expertise in the field of selection and development of data acquisition systems have been significantly helpful for the accomplishment of the project.

Similarly, I would like to thank Mr. Paul Ehrlich from BESTECH Australia Pty. Ltd for the genuine suggestion and guidance for the selection of the appropriate sensors applicable to the proposed model.

I would like to thank my fellow team members combinedly working as a team on the VAWT model especially Mr. Nitesh Poudel for developing the design of the Blade as per the requirement of my project.

I would like to humbly appreciate my family members and friends for all the enormous support throughout this time.

LIST OF FIGURES

LIST OF TABLES

ABBREVIATIONS

Abbreviation	**Definition**
VAWT	Vertical Axis Wind Turbine
FEA	Finite Element Analysis
DIC	Digital Image Co-relation
FBG	Fibre Bragg Grating
VPG	Vishay Precision Group
ADC	Analog to Digital Convertor
ESP	Express if Systems
R&D	Research & Development
PLA	Polylactic acid
GOBLET	Gauges of brilliant lifespan and Environmental Thoughtful
Symbols	**Definition**
V_0	Differential Output Voltage in Wheatstone bridge Circuit
V_{EX}	Excitation Voltage in Wheatstone Bridge Circuit
K	Gage Resistance
$\in$	Strain-induced
$\in_{max}$	Maximum Principal Strain
$\in_{min}$	Minimum Principal Strain
σ_{max}	Maximum Principal Stress
σ_{min}	Minimum Principal Stress
γ_{max}	Maximum Shearing Strain

ζ_{max}	Maximum Shearing Stress
E	Young's Modulus of Elasticity
v	Poisson's ratio

CHAPTER ONE INTRODUCTION

In this 21st century, the energy crisis has been one of the global concerns for the whole world. There have been numerous research and developments currently going for the solution to the energy crisis. The major concept of minimizing the global energy crisis is the generation of electricity using the renewable natural resources available. Wind energy has been one of the impeccable renewable sources for the generation of electricity contributing to 7.33% of the world's electricity generation in 2022 (Fernández, 2023). Wind energy is a clean and emission-free source of electricity generation.

1.1 Background of the project

The project is carried out in collaboration with Flinders University and VAWT-X Energy. VAWT-X Energy is one of the leading companies in South Australia primarily focused on the certification and commercialization of vertical axis wind turbine models patented with two-bladed air-foil technology. It aims to innovate a cost-efficient and aesthetic VAWT model providing sustainable energy alternatives to national-grid lines, and corporate and domestic consumers in Australia. (Energy, n.d.).

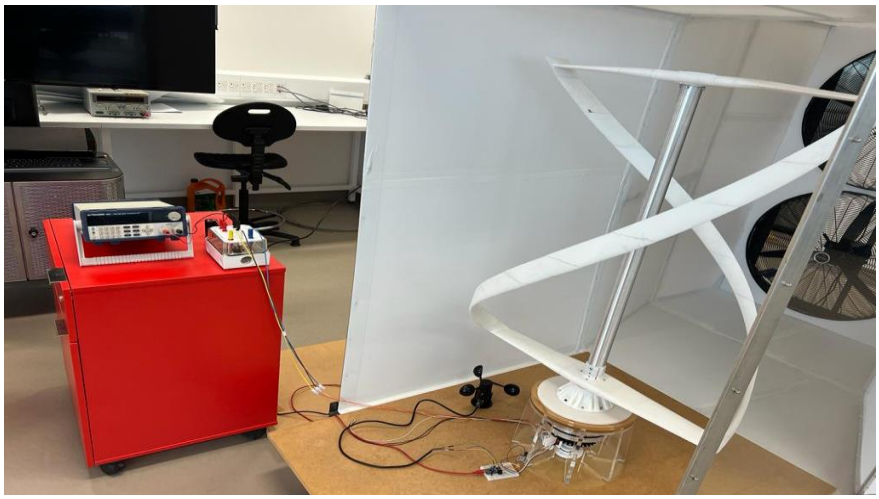

Figure 1: Existing VAWT model in Flinders Laboratory

There is the existing helical-shaped Darrius model of the Vertical axis wind turbine model present in the lab of Flinders University. This prototype of VAWT consists of two vertical profiles of blades designed with air-foil technology with sectionized 3D-printed blades. Different testing and certification have been carried out in collaboration with VAWT-X and Flinders University with the modification in this prototype. Each of the blade's profiles has been created with the concept of sectionized blade assembly. Each single vertical blade profile consists of the assembly of 9 sectionized blades.

The experimental measurement of the stresses and strain developed along the surfaces of the blade is a very challenging and complex task. The major issues arise due to the very compact and complex shape of the blades, the overall profile of the blades, and the connecting systems of the VAWT model. The presence of centrifugal forces during the rotational motion of the VAWT model limits the application of various commercial devices for stress and strain measurement. Moreover, the stress and strain measurement is further complicated by the high rotational speed of the VAWT model. Therefore, the experimental measurement of stress and strain is a pivotal aspect of every testing of the prototype yet there are numerous challenges within it.

The project is solely focused on establishing the concept of the stress and strain measurement system, particularly for the existing VAWT blades. With this accomplishment of the project, the testing methodology for ongoing and future VAWT-X projects would be enhanced. Therefore, the project upgrades the testing with a stress-strain parameter. The results obtained from such a measurement system would be able to predict the nature of stress and strain developed in the targeted and concerned area of the blade profile and therefore predict the lifespan and nature of the assembly in the long run. The design integration of the components of the measurement system should be minimal on weight and aerodynamical performance of the blade assembly.

1.2 Objectives of the project

The project is solely aimed at the identification and development of the appropriate stress- strain measurement system for the rotatory VAWT blades capable of fitting inside the compact geometry of the VAWT model and providing the wire/wireless transmission of the strain data. The system should adhere to the major system requirements declared by the stakeholders especially low-weight, cost-efficient, simple in construction, and simple to use in the VAWT blades providing wire and wireless transmission of data. With this aim of the project, the following objectives were defined:

1. To identify the suitable stress and strain measurement system with the comparative analysis of different methods in terms of system requirements described by stakeholders.
2. To design and identify the data acquisition system concerning the selected measurement system.
3. To identify the mathematical and theoretical framework for the data interpretation and analysis.
4. To identify the mechanical layout for the integration and installation of the measurement system within the complex VAWT model.
5. To carry out the experimental analysis of the measurement system on the VAWT blades along-with the verification by FEA analysis.

1.3 Scope of the project

The project is entirely focused on the design, development, and experimentation of the stress and strain measurement system for the Vertical Axis Wind Turbine Blades present in the laboratory. The project clearly defines the sole focus on identifying and selecting an appropriate measurement system applicable to the VAWT model. The project focuses on the selection of the appropriate data acquisition system and then identifies the mathematical and theoretical framework upon which output data would be interpreted. The project also identifies the concept of how each component is positioned and integrated within the VAWT model. The project carries out the experimental stress analysis on the VAWT blades and is validated with FEA analysis.

However, the design of new modified blades for the application of the measurement system would be kept beyond the scope of the project. The new profile of the blades for the application of the project would be derived from the parallel thesis project carried out under the same VAWT-X model. The re-design and structural modifications especially the upper spokes of the VAWT-X model require deep research to maintain aerodynamic integrity. Concepts of the joint of spokes and new blade profile could be another research field. All these structural modifications and re-design works have been kept beyond the scope of the project. Therefore, the project solely focuses on the design, development, and experimentation of a stress and strain measurement system for the Vertical Axis Wind turbine blades rather than the whole model.

1.4 Thesis Outline

Chapter 1 explains the background, specific problem encountered, the significance of the project, objectives of the project, its scope, and limitations. Chapter 2 provides the study of different journal articles and research papers for different stress measurement systems, data acquisition, and data analysis methods existing concerning the VAWT model. Chapter 3 explains a full description of the methods and activities using strain gages, their appropriate data acquisition system, the determination of the mathematical and theoretical approach for the data analysis, the design layout of the measurement system in the complex VAWT model, the procedure of development of the test model and FEA analysis. Chapter 4 explains the results of the testing of the developed test model under different loadings and its validation with FEA analysis. Chapter 5 provides the conclusion of the project along with the future endeavors that can be carried out in the project.

CHAPTER TWO LITERATURE REVIEW

2.1 Introduction

The design and development of the stress and strain measurement system for the Vertical Axis Wind Turbine Blade requires a foundational level of understanding of the various forces generated on the surface of the blade of the turbine in both static and dynamic loads. The study of different types of forces generated in the blade profile of the VAWT relates to the magnitude, direction, and relation of stress and strain along the blades. Next, the comprehensive understanding and comparison of the different stress and strain measurement systems applicable to Vertical Axis Wind Turbines provide the foundation strategy for the selection of an appropriate system for the proposed model. There is a paramount necessity of identifying the different types, specifications, advantages, and limitations of each measurement system along with the configurations, necessary accessories, and equipment required for the measurement. The study of the mathematical approach related to each system, and its applicational requirements provides the basis of the experimentation. The study of the data transmission system, data acquisition system, and interpretation approach is another challenging aspect that is required to be addressed before the selection of the system. With that, an appropriate research gap has been established. Each of these aspects is an integral part of the literature review for the project which is discussed in the following headings.

2.2 Different Forces & stresses acting in the blades of VAWT.

The blade profile of the wind turbine is the major critical component of the whole system. The curved blade profile of the wind turbine is subjected to various forces both under static and dynamic loading conditions. The wind turbine blades are subjected to major forces like aerodynamic lift and drag forces, centrifugal forces, gravitational forces, Inertial forces, fatigue loads, dynamic and turbulence loads, tower shadow, and wake effects. The blade profile of the wind turbine rotating under operation experiences lift and drag aerodynamic forces in a combined form. The direction of the lift force due to the impact of the wind speed is always perpendicular to the direction of the wind speed (Li, et al., 2015) . This lift force is the major driving force of energy conversion in the wind turbine. The drag force is also generated in a parallel direction with the wind speed which acts as resistance to the motion. There is the existence of centrifugal forces with the rotational speed of the blade which acts outward away from the rotational axis (Li, et al., 2015). The presence of centrifugal forces creates radial stresses on the blades and are proportional to the mass, length, and speed of the blade profile. Next to it is the presence of the gravitational forces caused by the weight of the blade which is

responsible for the bending moment along the extreme tip section of the blade as well as the base root of the blades. Next to these, there is also the presence of inertial forces in the blades of the wind turbine blades. The continuous acceleration and deceleration of the rotating blades of the turbine during its operation create additional stress along the blade profile due to the inertial stress. In addition, after a long time of cyclic loading, the blades of the wind turbine generate fatigue loads due to frequent changes in wind speed, wind direction, and even the dynamic response of the blades. The presence of fatigue loads is responsible for the degradation of the profile of the blade and deformation in the profile after long cyclic loading (Thomsen & Sorensen, 1999). The wind turbine also experiences dynamic loads in the form of vibrations caused by the turbulence of the wind speed which suddenly changes the values of aerodynamic forces in the blades (Thomsen & Sorensen, 1999).

Figure removed due to copyright restriction.

Figure 2:Forces on the VAWT blades (Li, et al., Effect of number of blades on aerodynamic forces on a straight-bladed Vertical Axis Wind Turbine, 2015)

With the loadings on the turbine blades, the surface of the blade experiences different forms of stresses and strains as per the loading orientation. (P.Sadanandam, Reddy, & Timmapuram, 2021). With the application of the bending forces, there is the generation of the three major stresses namely tensile stress, compressive stress, and shear stress. Tensile stress is generated along the surface where the material is stretched away normally on the convex side under bending forces, whereas compressive forces are generated on the concave side causing contraction of the materials. Shear stress acts along the cross-section of the blades (P.Sadanandam, Reddy, & Timmapuram, 2021). Under the application of the multi-axial loadings, there are axial stress, shearing stress, torsional stress, and bearing stress generated on the surface of the blades. (Yu, Zhu, Liu, & Liu, 2017). Axial stresses are generated along the length of the blades under axial loading. Torsional stresses are generated with the presence of

torque and bearing stresses are generated at the point of contact or support. (Yu, Zhu, Liu, & Liu, 2017). These stresses are the key factors that affect the performance and efficiency of the blades. If the developed stresses are under the ultimate strength level of the material of the blade, the material selection can be considered safe for practise. These stresses are the key factors that determine the integrity of the whole system, especially at the points of connection and support. The calculation of these stresses and strains would help to predict the lifespan and any case of failure. With the calculation of these stresses, the major performance criteria of the turbine system like speed limitation, design limitation, connection, assembly, etc. can be enhanced for the best performance of the turbine.

2.3 Historical Development of Stress & Strain Measurement System in Wind Turbine Model.

The discovery of the Wheatstone bridge circuit in 1833 by Samuel Hunter Christie and improvised by Sir Charles Wheatstone in 1843 was the revolutionary milestone in strain measurement. This system allowed to show the change in resistance in the conductor under the application of mechanical stress which results in the change in the differential voltage in the Wheatstone bridge circuit (Hoffmann, 1987). This concept has been the foundation for the application of different strain gages like metal foil strain gages developed in the 1930s till date. In the Wheatstone bridge circuit, the strain gage is connected to 3 fixed resistors. A balanced Wheatstone bridge is the condition that the voltage difference across the bridge is obtained to be zero. It can be obtained if the ratio of consecutive resistors in the Wheatstone circuit is equal. With the balanced bridge condition maintained initially, any change in resistance of strain gage caused by deformation, the bridge is unbalanced and there is a generation of voltage across the bridge which can be used as a measure of calculation of stress and strain caused by the deformations.

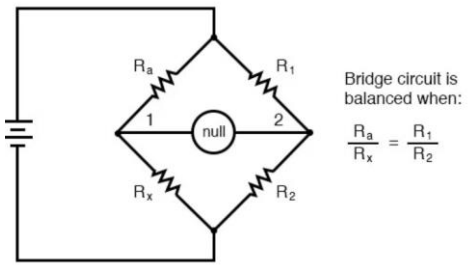

Figure 3: Balanced Wheat-stone Bridge circuit

With the development in technology, the measurements of strain-induced were allowed to be measured with different materials like semiconductors, optical fiber, etc. throughout the late 19th century. With the significant growth in technology, different advance stress and strain measurement systems like Fibre Bragg Grating sensors, digital image correlation, and miniature

strain sensors were introduced. The strain measurement and pattern recognition in the blades of the wind turbine were experimentally carried out for the blades of the wind turbine basically with two major methods namely fiber optical sensors and strain gauges (Pérez, Torres-Arredondo, & Güemes, 2015). In this paper, they embedded two types of fiber optics sensors namely Fiber Bragg Gratings (FBGs) and Optical Backscatter Reflectometer in the 13.5m wind turbine made of glass fiber and vinyl-ester resin. Strain Gauges were also bonded to the surfaces of the wind turbine. 4 optical fiber sensors having 6 fiber Bragg gratings were embedded in the blade of the wind turbine whereas several strain gauges were also bonded to the surface of the blade profile and definite known loads were applied to the cantilever blade profile to analyze the strain patterns with the determination of strain level incorporating squared predicted error method (Q-index and T^2-index). Strain measurement and pattern recognition using different sensing methods were able to detect deformations and non-linearities properly. (Pérez, Torres-Arredondo, & Güemes, 2015). The optical fiber sensors demand the application of loading before the testing and its accuracy is more in the presence of the distributed sensing. The FBGs over strain gauges are robust and possess electromagnetic immunity to the longest life as the FBGs are engraved in Optical fiber sensors inside the blade profile which is not feasible for VAWT blades. However, Strain gauges being simple in construction and nature are equally capable of synthesizing the same strain measurements. Strain gages are capable of being bonded to the surface so require no prior embedding while manufacturing and are flexible to place at any required points of concern (Pérez, Torres-Arredondo, & Güemes, 2015).

According to the conference proceedings of the Society for Experimental Mechanics Series 27 held in 2012, the strain and stress measurement for the dynamic loading conditions in the wind turbine blades was executed by the comparative performance analysis of Digital Image Correlation (DIC) and strain gages. Digital Image Correlation requires special high-speed cameras and software named Aramis for stress analysis (Carr, Baqersad, Niezrecki, Avitabile, & Slattery, 2012). In this experiment, a 5 ft long rectangular cross-section Aluminium beam was clamped with fixed support to create a cantilever beam. Two dynamic tests were performed, first, a pluck test in which the tip of the beam was given a displacement to oscillate and the second included the use of a shaker on the base of the beam to create the oscillation in the beam measuring strain values against time. (Carr, Baqersad, Niezrecki, Avitabile, & Slattery, 2012). The paper clarifies the DIC was capable of measuring full-field stress and strain along the whole surface of blades on dynamic testing, but the strain gauge was limited to the specified point being bonded. However, the paper confirms the similarities and coherence of the results of both mechanisms. The impacts of noise in the calibration using DIC techniques and the nature of system arrangement for executing DIC is one of the issues over the application of DIC in

rotary VAWT models. The use of DICs in the rotatory VAWT blade conditions along with the influence of noise and vibrations seems more complicated and complex. The use of DIC in rotary systems like the VAWT model is also limited by the system requirements for high-resolution images and a limited field of view. The strain gages being simple in construction and geometry were still capable of detecting the stress and strain to the closest accuracy to the High tech like DICs. (Carr, Baqersad, Niezrecki, Avitabile, & Slattery, 2012).

The use of the strain gauge has been traditionally approved for the measurement of static as well as dynamic loading conditions. They are simple in design and construction and require a small space along the surface of measurement usually bonded on the surface of the material using the adhesives and powered with the electrical distribution. The use and capability of the strain gauge for the measurement of the strain near the tip of fracture and failure are highlighted by the research paper (Dally & Sanford , 1987). It explains the complexity of the measurement of the strain near the crack and demonstrates the application of the strain gauge for the measurement of the stress-intensity factor in the plane body having a crack. The paper suggested the impact of the proper selection of strain gradients and the position and orientation of the strain gauge for such conditions (Dally & Sanford , 1987) The paper suggested three major approaches to measure the stress intensity factor at the crack tip namely single gage-three parameters, two gage- four parameters solution, and the use of rosette strain gage. The paper showed the importance of the orientation of the single or double strain gauge for precise measurement and revealed a rectangular rosette strain gauge for the very purpose (Dally & Sanford , 1987). It can be seen the results of strain measurements by strain gauge are solely dependent on the selection of the position and orientation of its installation. Strain gages can detect the deflection over a limited area of surface within its gauging area.

Therefore, the selection of strain gage particularly rectangular rosette strain gage for the measurement of stress and strain in the VAWT blades is selected with the comparison carried out with the decision matrix reading above research papers addressing the major system requirements in the VAWT models.

2.4 Different Strain Gages and its configuration

The application of the strain gauge for stress and strain measurement has been one of the traditional yet most accurate, precise, easy-to-install, and cheap systems. Strain gages with different orientations and applications are available. The selection of the appropriate strain gage for the desired application requires the identification and selection of various parameters. The selection of the strain gage depends upon multiple parameters like the functionality of the strain gages, the material on which it is bonded, types of the grid geometry and gage pattern, bonding

adhesives, options of connection, etc (Micro Measurements-a VPG Brand , 2020). To be specific, there are standard parameters to be identified like gage series, self-temperature compensation number, gage length, gage pattern, gage resistance, types of measurements, bonding adhesives, longevity, and calibration requirements. (Micro Measurements-a VPG Brand , 2020). The parameters describe respectively the type of measurements like static, dynamic, and post-yield analysis, the nature of materials in which strain gages are to be installed, the range of temperature compensation required by the gages, the gradients and area of maximum strain to be measured, biaxiality of stress and pattern of metal foil required for measurement, resistance and heat dissipation nature of gage, soldering and installation requirements, adhesives and cure temperature, external contamination and calibration methodology of the strain gages. The gage series like CEA, EA, CHA, etc which present strain gage series for general-purpose applications like static and dynamic applications can measure strain due to bending, torsion, shear, and thermal change (Micro Measurements-a VPG Brand , 2020). Having a high gage resistance allows for the minimization of the effects of lead wires in series and improves the signal-to-noise ratio. The high gage resistance also provides the advantage of the use of high excitation voltage minimizing grid self-heating (Micro Measurements-a VPG Brand , 2020).

However, the commercially available strain gages are normally categorized based on the orientation of the gage pattern. There are normally four gage patterns of the strain gages linear, shear, and Torque patterns, Tee Patterns, and rectangular rosette patterns (Brand, n.d.). Linear Patterns are used for the measurements of the strain in the single specified directions with normally single-grid and parallel dual-grid patterns for general-purpose applications like fatigue testing, concrete testing, crack propagation, etc. Shear and Torque strain gages are usually deployed to measure the shear strain caused by the application of the Torsional loads. These patterns are normally oriented in ±45°to the direction of measurement along the shafts (Brand, n.d.). Tee patterns are usually used for the application of direct tension measurements and bending applications. Rectangular rosette strain gages, having three strain gages oriented in 0°,45°, and 90° are usually used for general uses like tension, compression, and bending measurement but typically where principal directions are unknown. (Brand, n.d.) which is the best type for the application.

2.5 Calibration System Concerning Strain Gages

Strain Gages are the key element that relates the strain induced by the deforming load to the change in resistance of the metal foil and gridlines in strain gages. Strain gages are incomplete with the supply of the Wheatstone bridge circuit. These are the passive elements in the whole

measurement system that require input power for operation. There are three major configurations namely quarter bridge circuit, half-bridge circuit, and full-bridge circuit the strain gages can be connected to (Lab., 2021). The quarter bridge circuit is the connection of one active strain gage with three other fixed resistors. This bridge circuit is simple in construction and can be used where temperature compensation is negligible (Lab., 2021) Similarly, Half bridge circuit consists of two active strain gages with two fixed resistors and is much more sensitive than the quarter bridge system towards the effects of the temperature on the strain gages. A full Bridge circuit uses four of the active resistances and is sensitive to any fluctuations in temperature compensation (Lab., 2021). Therefore, temperature compensation plays a vital role in the selection of the appropriate bridge circuit for the strain gage. For simple and precise construction in compact VAWT blades, a quarter bridge circuit seems to be the best available method from this literature.

2.6 Data Acquisition System Incorporating Strain Gages

The differential output voltage change in the Wheatstone bridge circuit caused by the application of the loads is very small in amplitude (Hoffmann, 1987). These Analog signals are small in magnitude and can therefore easily be overshadowed by external disturbances, vibrations, and noises. So, without any signal conditioning system, the data measurement would always be inaccurate. Therefore, to eradicate the influence of external disturbances and noises, there is a necessity of amplification of the signals. The analogy signals from the bridge circuit can be amplified with some signal amplifier with a gain factor to a level that dominates the external noises and disturbances. Then, the amplified signals can be forwarded to an analogy display, recorder, or counter and even with a digital display. There is also the possibility of the use of electronics to enhance and optimize the data acquisition system of the strain signals.

The measurement and acquisition of the data can also be carried out in digital form with the use of simple electronics. The strain gages with its Wheatstone bridge circuit provide the weak Analog signals having the strain data. This data can be first amplified using an amplifier with some desirable gain factor. Then the amplified Analog data can be converted to digital signals using an Analog-to-digital converter (ADC). There are different models of ADCs that are capable to amplify and digitalize the signal in the same system (Anderson Langone, et al., 2018) . The digital signal provides the advantage of being resistant to any kind of external noise and disturbances. The digital signals are then forwarded to data acquisition systems like Arduino Uno board, ESP-8266, ESP-32, etc (Anderson Langone, et al., 2018) The data acquisition system now requires the use of programming platforms like Arduino, Python, C++, etc. to extract the digital values of the Analog strain signals (Anderson Langone, et al., 2018) . In this paper,

strain gage is connected to a Wheatstone bridge configuration having Nanoshield LoadCell to facilitate the connection and Arduino Mega2560 as the micro-controller. The system is facilitated with an amplifier, a filter, and a 20-bit ADC for signal conditioning. The paper suggested the use of this method to have good efficacy in applications with satisfactory accuracy carrying the experiment in the cantilever position for the blade. The data can be displayed in the form of graphs and can also be interpreted in terms of voltage induced in the bridge and the values of the strain and stress generated in the strain gage using the theoretical and mechanical principles. Such systems are very simple in construction and experimentation also provides the advantage extremely low-cost data acquisition system. This electronics method can provide precise and accurate stress and strain measurement in comparison to other traditional strain measurement systems (Anderson Langone, et al., 2018).

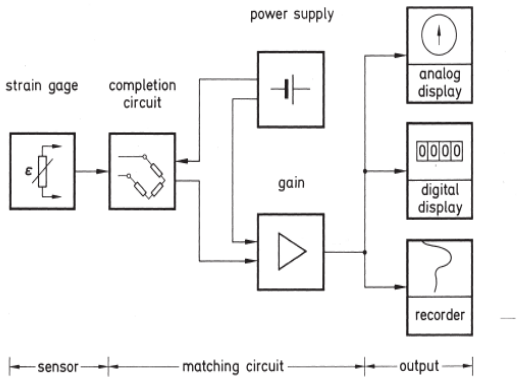

Figure 4: Data Acquisition System Using Strain Gage Configurations

The use of an electronic data acquisition system seems to be a very convenient approach to achieving the project objectives underlining the stakeholders' and system requirements especially lesser weight, lesser space consumption, low cost, simple in use, flexibility of wire/wireless data acquisition system and being able to fit in compact geometry of VAWT blade and system itself.

2.7 Gap Statement

VAWT model is complex and compact in the sense that 9 sectionized blades are assembled to create each helical curve blade profile and different other mechanisms are installed within the confined space. There has been limited experimental stress analysis carried out in a rotatory system like the VAWT model. The appropriate stress and strain measurement for the VAWT model should fulfill the major system requirements mentioned by the stakeholder weight, simple in construction, capable of wire and wireless data transmission, simple in use, and more importantly flexible to fit in the compact blade geometry of the VAWT blade and model itself.

The appropriate stress measurement system is to be selected based on the following metrics or system requirements. The experimental stress measurement provides the capability of instant and live measurement of stress under different testing phases that would be carried out for the improvement of the VAWT model in the future rather than the repeated theoretical approach of measurement. With the study of various literature reviews, the use of a strain gauge with an electronic data acquisition system should be the best optimal solution to the selection and development of a stress and strain measurement system, particularly for the VAWT model. It is found that limited experimental analysis has been carried out with the use of a strain gauge and the design of a simple and compact data acquisition system using ADCs and microcontroller chips for a rotatory system like the VAWT model. The project would explore the design, development, and experiment of stress and strain measurement systems for VAWT blades using strain gage and compact data acquisition systems comprising ADCs and microcontrollers.

CHAPTER THREE METHODOLOGY

3.1 Introduction

With the required research and investigations from the published journal articles, literature reviews, case studies, and research papers, the appropriate methodology to be followed to meet the project objectives was identified. This chapter discusses in detail and depth sequence of methods carried out to meet the project objectives. This chapter initially describes the type of stress-strain measurement system deployed for the VAWT blade, its specifications, and its configurations. Secondly, it describes the mathematical and engineering theory and laws to be applied for the evaluation and analysis of input/output values of the measurement system. Sequentially, the chapter progresses on the description of the appropriate data acquisition system installed in the project. Then, the chapter describes how all these measurement entities and components would fit in such a complex and compact existing VAWT model. The chapter describes each step executed in the development of the test model and the testing.

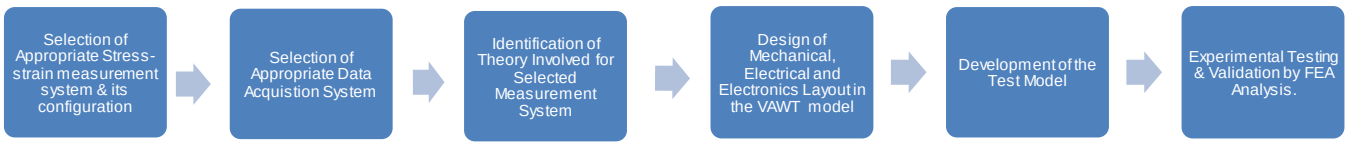

Figure 5: Flow Diagram of Project Execution

3.2 Selection of Appropriate Stress-Strain Measurement System & its configurations.

The study and investigation of different research papers provided the use of different stress-strain measurement systems applied for the wind turbine blades including fiber optic sensors, digital image correlation, acoustic sensors, and strain gages. With the precise study of each of the measurement systems and their specifications, a decision matrix (See **Appendix A**) was created, it was found that strain gage is extremely predominant in other methods as it is low-weight, simple in construction, and use, flexibility to fit inside VAWT model and scope of introducing wire/ wireless data transmission.

The rectangular rosette strain gage is the type of strain gage having three individual strain gages having similar gage grids closely positioned and separately oriented in three different directions i.e. °,90° and 45° to measure normal strains along each direction in the underlying surface of the test specimen. Strain gage elongates or contracts upon deformation and loadings resulting in the change of resistance. The rectangular rosette strain gage was selected as it addressed the issue of major principal directions in the curved blade surfaces of the VAWT blade being unknown. To add value to the statement, rectangular rosette strain gage provided strong attributes in fulfilling the major requirements of the strain measurement like universal general-purpose static and dynamic stress analysis, efficient to various forces like tension, compression, bending, and moments, and more importantly applicable to 3D printed material like PLA.

With these attributes, the model ‘FRAB-1-11-1LJB-F’ a rectangular rosette strain gage was selected and procured from BESTECH Australia Pty. Ltd. The model is marked with the GOBLET logo which stands for ‘Gauges of brilliant lifespan and Environmental Thoughtful’. The model is also CE marked and compliant with RoHS2 Directive 2011/65/EU standard. The specifications of the model ‘FRAB-1-11-1LJB-F’ are listed. (See in Appendix B)

The rectangular rosette strain gage of gage resistance 120Ω is selected with the vision of higher flexibility and compatibility of connections to a standardized acquisition system and an even simpler bridge circuit. It generates less self-heating under low-voltage power sources. Having the gauging length and width of 1mm and 0.7mm respectively, the strain gage provides a resolution of 1/1,000,000 with a strain limit of 5% at room temperature and fatigue life strain level of ±1500 μ∈. Having a higher gauge factor of 2.06 (greater than 2) provides evidence of higher precise, accurate, and highly sensitive strain gauge capable of generating ample change in electrical resistance with the smallest loads and deformation. This value of the gage factor is also responsible for enhancing the signal-to-noise ratio reducing the effect of external electrical

noise and disturbance. The temperature compensation of 11*10^-6 /°C is well suitable value to compensate for any deviations caused by the temperature change.

3.2.1 Design of Quarter-Bridge Circuit Configuration

As discussed in the Literature review about different bridge configurations available for the strain gages, a Quarter bridge circuit configuration was selected for the bridge completion. The major reasons for the selection of the quarter bridge circuit to be connected to each of the strain gages in the rectangular rosette strain gage were its simpler construction and versatility to connect with a wide range of instrumentations. The cost of installing the quarter bridge circuit was also highly economical because of the use of readily available 120 Ω fixed resistors and simpler construction and installation.

The construction of the quarter bridge circuit was carried out with the procurement of two major key components.

i. Thick film Surface Mount Resistor of 120 Ω

A thick surface mount resistor of 120 Ω was selected for the resistors of the quarter bridge circuit. They require very small space for installation and are small in weight and therefore flexible for VAWT blades. These fixed resistors having a resistance of 120 Ω with a minimum tolerance of ±1% are selected to create a balanced quarter bridge circuit (See Appendix B, Table 6)The selection of the resistance of 120 Ω and power rating of 0.25W would generate an individual voltage that is acceptable to the excitation voltage supplied to the passive strain gauge and its bridge configuration.

ii. Strain Gauge Connecting Terminals Type TF-2SS

The connecting terminals provide the proper and convenient junction points to allow the connection of the strain gages to the instrumentation lead wires. The type TF series is built with 0.03mm thick copper foil and a glass-epoxy insulation base of 0.15mm thick suitable for soldering thick surface mount resistors. The major specification of the TF-2SS is listed in Appendix B, Table 7.

Quarter bridge circuits were developed using a thick film surface mount resistor of 120 Ω with the smallest available tolerance of ±1%. With the selection of the smallest tolerance limit of resistance of the resistor, the issue and error caused by the unbalancing of the wheat-stone bridge were negligible. However, the calculation of stress and strain in the project is based on the voltage difference generated before and after the loading stage which can be obtained through the change in digital signals under loading. Therefore, the balancing of the Wheatstone

bridge wasn't considered into account which was later considered to be a major limitation of the project.

3.3 Selection of Appropriate Data Acquisition System

A Data Acquisition System can be defined as a specialized combination of hardware and software dedicated to the collection, measurement, processing, and storage of data from different sensor systems. The design of the Data Acquisition System is required for the monitoring, control, and analysis of the measurement.

The concept of the wired communication of the strain gages whole along the blades, shaft, and base structure of the model to the stationery base station positioned close to the model provided serious issues in technical aspects. The major issues encountered during the development of wired communication for the VAWT model are listed below:

i. The use of long lead wires for strain gages and the too-long connecting wires carrying Analog signals from strain gages to the stationery instrumentation would be highly influenced and degraded by external electrical noises and disturbances. The generated Analog signals are very small in amplitude and practically influenced by external noises and vibrations.
ii. Having the long-wired communication would indirectly cause self-heating of the system and thermal drifts along the path.
iii. The signals from the wired communication would highly be polluted by all of these factors resulting in inaccurate and false measurements.

3.3.1 Concept of Wireless Communication for the VAWT Model

To resolve above mentioned technical issues, the concept of a wireless communication system was approved. The concept design of wireless transmission of the strain signals to a stationery base station is very intriguing. The concept of wireless transmission of the data would eventually resolve the issue of long and complicated wired connections in a rotatory system of VAWT. The wireless transmission system also resolves the issue of strain data being corrupted by external disturbances and noises with the concept of amplification and digitalization of the signals. The transmission by wireless mode demanded the use of simple electronics configurations comprising as listed:

i. Adafruit NAU7802 24-Bit ADC - STEMMA QT / QWICC
ii. Spark Fun QWICC Mux Breakout - 8 Channel (TCA9548A)
iii. Spark Fun Thing Plus - ESP32 WROOM (USB-C)
iv. 3.7V 2000mAh LiPo battery

v. **Flexible QWICC Cable - 50mm**

vi. **USB 3.1 Cable A to C - 3 Foot**

vii. **Arduino Programming**

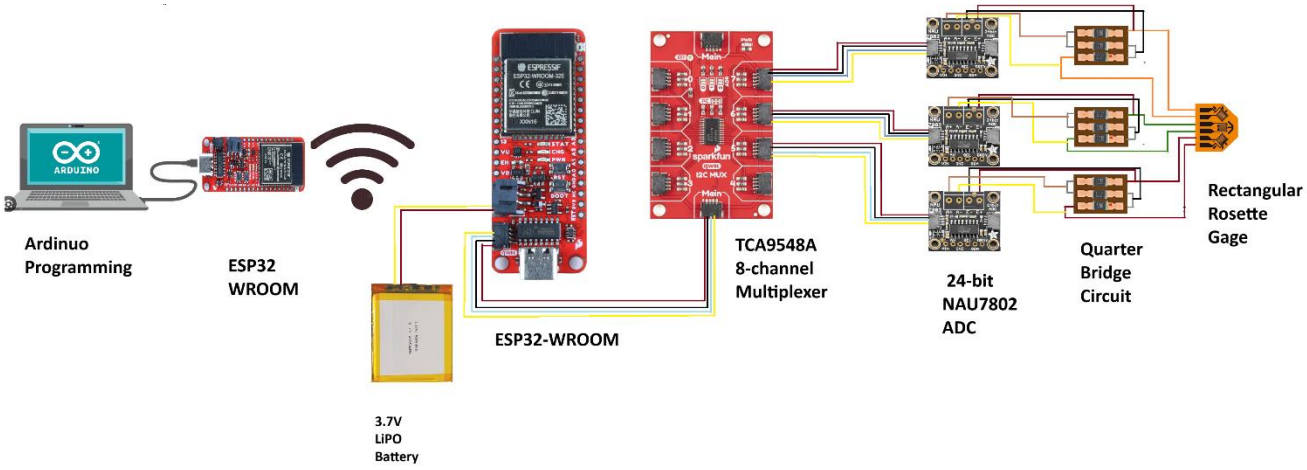

Figure 6: Wiring Diagram of the Whole Measurement System

The concept of wireless transmission is shown in the following figure and explained in detail.

i. Adafruit NAU7802 24-Bit ADC - STEMMA QT / QWICC

This 24-bit Analog digital converter is the first key element connected to the strain gage & its quarter bridge connection. This component carries the dual function of amplification of the signals and digitalization of those Analog values. The main purpose of this component can be highlighted as

a. It converts the Analog voltage values obtained in the quarter bridge under the application of the strains and deformations into the form of digital output values along with the amplification of the signals.
b. The output signals from this component are amplified and digitalized which resolves the issue of corruption and degradation of the signals from external electrical noises and disturbances.
c. Having the 24-bit ADC, the component provides very high resolution as the Analog signals would be represented in 2^24 i.e., 16,777,216 discrete levels thereby ensuring the precise measurement of the strain and voltage induced.
d. The use of 24-bit ADC affects the signal-to-noise (SNR) ratio in the way it captures the large number of digital steps providing a better representation of the digital signals than 16-bit however it doesn't play a role in reducing noise.
e. This ADC is very compact and small which can be justifiably positioned in the existing VAWT model.

f. It enhances the sensitivity to capture very small changes in input signals with precise control and efficient data acquisition.
(nuvoton, NAU7802 24-bit Dual-Channel ADC For Bridge Sensors , 2012)

ii. Spark Fun QWICC Mux Breakout - 8 Channel (TCA9548A)

This Multiplexer consists of 8 channels for the connection of multiple sensors under the same bus. Each of the ADCs as discussed above has the same fixed I2C address. So, to communicate with multiple sensors having the same fixed I2C address under the same bus, this QWICC MUX breakout board is selected. The key features for the selection of this component can be highlighted under the following points.

a. It allows multiple sensors with fixed I2C addresses to communicate in the same bus.
b. This board consists of eight configurable addresses which can be used for a maximum of 64 I2C buses.
c. It provides all the communication enabled through I2C exclusively making it very user-friendly and easy to use.
d. The operating voltage of this board is in the range of 1.65V to 5.5V which is perfectly compatible with the project execution.
e. It provides a 4-pin JST connector to the board allowing communication through 4-pin JST connector. (Instruments, 2019)

The reason for using an 8-channel multiplexer can be explained. One rectangular rosette strain gage is made of three individual strain gages. Each strain gage is provided with individual quarter bridge circuits which are again individually connected to each 24-bit ADC. This can be easily visualized from the wiring diagram presented above in Fig. 6. In application to the VAWT model, there are two blade profiles in the model. The use of two rectangular rosette strain gages in each of the blade profiles of the VAWT demands a minimum of 6 ADCs connected to 6 channels in the multiplexer so that all the communication can be carried out in the same bus. Therefore, an 8-channel Multiplexer breakout board is selected for the application.

iii. Spark Fun Thing Plus - ESP32 WROOM (USB-C)

The ESP32 WROOM Things Plus with USB-C has been one of the integral parts of the Wireless Communication and Data Acquisition System. The ESP32 WROOM Things Plus with USB-C is a powerful microcontroller module that facilities the Wifi and Bluetooth features exclusively. This ESP32 allows communication with the 8-channel Multiplexer previously discussed through one QWICC connector.

The key features of this ESP32 WROOM with USB-C model can be highlighted as

a. It exclusively provides Wi-Fi & Bluetooth features with an integrated antenna for the transmission of the data.
b. It provides a 2-pin JST connection for the LiPo battery which simplifies the connection and installation.
c. It provides the QWICC connection system which eliminates the soldering and connection workloads.
d. It provides the facility of USB-C connection which can be used for the connection to a computer.
e. It supports programmable platforms like Arduino IDE and other environments. (Systems, 2023)

For the execution of the project, two ESP32 WROOM modules are being used. The first ESP32 module is connected to the Multiplexer communicating with a 24-bit ADC configured to each of the strain gage sensors. This ESP32 module would be allocated in a justifiable position within the VAWT model. Therefore, this ESP32 would fit inside the VAWT model subjected to both static and rotational phases. This ESP32 module would act as the client model. It would transfer all the digital values from the strain gauge and its configurations wirelessly through its Wi-Fi and Bluetooth capabilities. Now, the role of the second ESP32 comes into play. This second ESP32 module would act as a receiver of those digital values from the first ESP32 module. This second ESP32 module would be connected to the computer through a USB-C cable and all the digital values would be extracted through Arduino Programming. Therefore, this second ESP32 module would be stationary and connected to a computer with a USB connection. The stationary ESP32 module would act as a server emitting Wi-Fi connections under its IP address and password. The first rotatory ESP32 would act as a client connected to that Wi-Fi connection and transmission of the digital output values would be carried out.

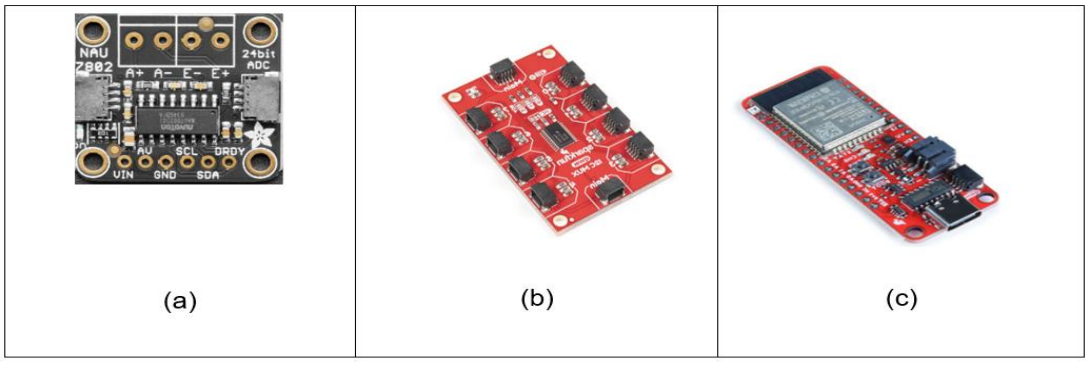

Figure 7: Electronics Components (a) 24-bit NAU7802 Analog to Digital Convertor; (b) TCA9548A MUX board; (c) ESP-32 WROOM

iv. 3.7V 2000mAh LiPo battery

The selection of the battery was carried out with the calculation of the power consumed by each of the electrical and electronics components. First, the operating voltages and operating current for each of the components were obtained from the datasheet of each of the components. Then, individual power consumption was calculated. Then, the total power consumed was determined and a suitable battery was selected. The power calculation for the selection of the battery is shown in Table 8 (See Appendix D). Considering the time of operation to be 4 hours, The battery capacity required is given by

Battery capacity= 0.228A*4hr= 0.912 ~ 1Ah battery.

Considering the effects of power consumption by the wirings throughout the circuit and losses, the factor of safety of 2 was considered. With that, a 3.7V 2000mAh battery was selected for the purpose.

v. Flexible QWICC Cable - 50mm

This QWICC cable, 4- a conductor cable having 1mm JST termination, was used for the connection of each ADC to the multiplexer. The connection of the multiplexer with the client ESP-32 module is also established using Flexible QWICC Cable.

vi. USB 3.1 Cable A to C - 3 Foot

This cable is used for the connection of the stationary ESP32 module (server) to allow the connection to a computer with the Arduino IDE programming platform.

vii. Arduino Programming

The software for the collection of the data and display of the testing and measurement was selected to be Arduino IDE. The programming and software are user-friendly and easy to use. Most of the components provide free source code for the execution and use of the component in the Arduino platform. The programming also facilitates the mode of providing the excitation voltage to the bridge circuit, the amplification gain factor of the ADC, sampling speed of the ADC during the testing and measurement. The software can be used for the display of the digital values of the strain signals obtained throughout the system. Then, the change in the digital signals can be used for the conversion and interpretation of the data into stress and strain values through the principles of stress and strain. The development of the code programming can be carried out for the testing of the system once built in both wired communication and wireless communication between two ESP32s.

3.4 Identification of Theory Involved in Selected Measurement System

The theory is based on the conversion of change of digital strain values due to loadings to the change in voltage in the bridge circuit then convert them to the values of stress and strain induced.

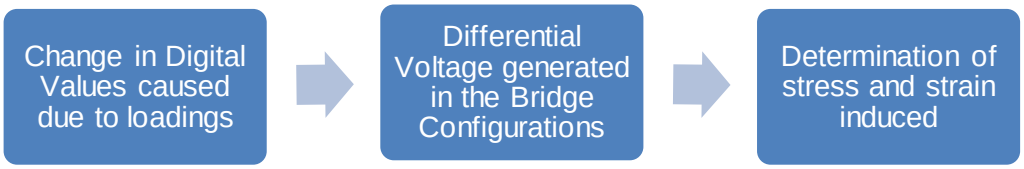

Figure 8: Flow-chart of data conversion and Mathematical Analysis

The theory can be expressed following points.

A. Conversion of Change in Digital Values caused due to loadings to the Differential Voltage generated in the bridge configurations.

This conversion majorly focuses on how ADC digitalizes the Analog voltage values to the digital values. There is a standard voltage reference level which is mentioned in the datasheet of the Analog to digital convertor. For 24-bit NAU7802 ADC, V_{ref} is 2.4V as mentioned in the datasheet of the NAU7802 ADC. It means that 2^24 discrete digital levels would be representing -1.2 to +1.2V.

2^24 discrete digital counts represent 2.4V (nuvoton, NAU7802 24-Bit Dual-Channel ADC For Bridge Sensors, 2012). i.e. 1 discrete digital count represents 1.430511*10^-7V. But as the digital value was amplified by the gain factor, to get the Analog voltage value, it needs to be divided by the gain factor set during the programming at the testing period.

This can also be represented by the following equation derived from the sources,

$$\textbf{Voltage value across bridge} = \frac{\textbf{Digital values}}{2^{n}-1} * \frac{V_{ref}}{\textbf{Gain}} \quad \text{.....} \quad \text{eqn (1)} \quad \text{(SparkFun, n.d.)}$$

Where, Δ Digital values= change in Digital values of ADC in the COM window,

V_{ref} = Fixed reference voltage of ADC = 2.4V (from datasheet of NAU7802),

n= number of bits of ADC i.e., 24 (24-bit ADC),
$2^n - 1$ = resolution of the ADC.

Gain = Gain of ADC set i.e., 64 set in programming

B. Conversion of Differential Voltage to Strain Values in Quarter bridge.

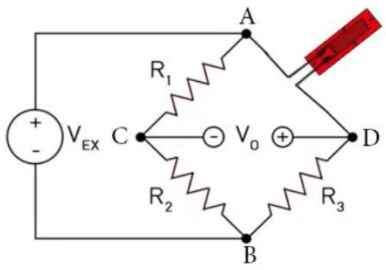

Figure 9: Quarter Bridge Circuit

Let R_1, R_2, and R_3 be the fixed resistor and R_4 be the resistance of the strain gauge. On loading and deformation, let the change in the resistance be ΔR.

The voltage at the point C = $\frac{R1}{R1+R2} * V_{EX}$ (Bestech, n.d.).

The voltage at the point D=$\frac{R4+\Delta R}{R4+\Delta R+R3} * V_{EX}$

The differential voltage output is

$V_0 = \left(\frac{R4+\Delta R}{R4+\Delta R+R3} * V_{EX} - \frac{R1}{R1+R2} * V_{EX} \right)$

For $R_1=R_2= R_3 = R_4 = R$,

$V_0 = \frac{VEX * \Delta R}{4R+2\Delta R}$

Now, since R>> ΔR and 4R>>2 ΔR;

$V_0 = \frac{VEX}{4} * \frac{\Delta R}{R}$

i.e. $\boxed{\mathbf{V_0 = \frac{VEX}{4} * K * \epsilon}}$ (Bestech, n.d.)

Where Gage resistance(K) =2.06 ; $VEX = 3V$

C. Determination of stresses in Rectangular Rosette Strain Gage.

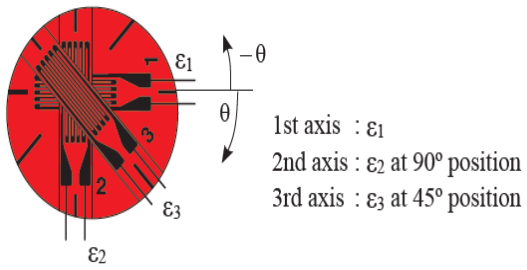

Figure 10: Rectangular Rosette Strain Gage

With the values ϵ_1, ϵ_2, ϵ_3 be determined from Step B which represents each of the strain gages of the rectangular rosette strain gage. The theories of Maximum principal stress and strains can be deployed to obtain each of the values of theoretical strains and stress.

Maximum Principal Strain: ϵ_{max}
$= \frac{1}{2} [\epsilon_1+\epsilon_2+\sqrt{2 * \{(\epsilon_1-\epsilon_3)^2 + (\epsilon_2-\epsilon_3)^2\}}$

Minimum Principal Strain: ϵ_{min}
$= \frac{1}{2} [\epsilon_1+\epsilon_2-\sqrt{2 * \{(\epsilon_1-\epsilon_3)^2 + (\epsilon_2-\epsilon_3)^2\}}$

Maximum Shearing Strain : γ_{max}
$= \sqrt{2 * \{(\epsilon_1-\epsilon_3)^2 + (\epsilon_2-\epsilon_3)^2\}}$

Maximum Principal Stress $\sigma_{max} = \frac{E}{1-\nu^2} (\epsilon_{max} + \nu \epsilon_{min})$

Minimum Principal Stress $\sigma_{min} = \frac{E}{1-\nu^2} (\epsilon_{min} + \nu \epsilon_{max})$

Maximum Shearing Stress
$\zeta_{max} = \frac{E}{2(1+\nu)} \gamma_{max}$ (Lab., 2021)

Stress Intensity = $\frac{E}{(1+\nu)} \gamma_{max}$ ((Data, n.d.)

where,

E= Young's Modulus of Elasticity 2.34 GPa.

Poisson's ratio (ν) = 0.35 for PLA. ((Data, n.d.)

3.5 Design of Mechanical, Electrical, and Electronics Layout in the VAWT model

The next challenge encountered was how the system would fit in such a compact, complex, and more importantly rotatory system. Therefore, determining the layout of how mechanical, electrical, and electronic systems would be positioned in the VAWT model without interfering with the aerodynamical performance of the system is a very critical aspect of the measurement system. The design layout should have minimal impact on the mass-balance along the shaft axis and a bare impact on the blade aerodynamic performance.

With that vision, the layout of the whole stress-strain measurement system had been designed and identified with minimum impact on blade aerodynamic performance and mass-balance along the central axis of the blade. The description of how mechanical, electrical, and electronic components are integrated and positioned is described in detail under the following sequence of points.

i. Design Modification of Existing Blade Profile.

The existing blade is modified with the new design of the blade having a hollow cavity supported by a Z-section along the blade profile. The newer design of the blade carried out in a fellow research project under the VAWT model also features the step lap joint for the connection of two sectionized blades. The hollow cavity is designed with the secondary aim of providing enough space for the wiring of the designed measurement system within the VAWT model. The hollow cavity is to be used for positioning the smaller electronics components of the system and also provide passage of wires along the VAWT model up to the top of the wind turbine.

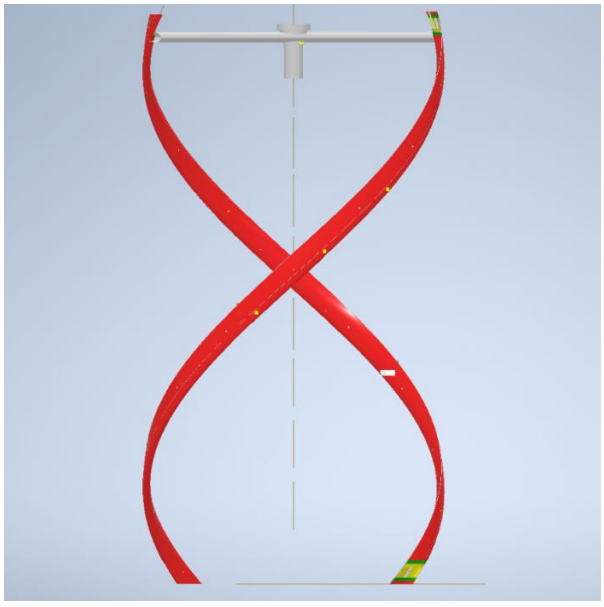

Figure 11: Assembly Drawing of the Designed layout of the Measurement System

ii. Determination of the positioning of the strain gage and its bridge configuration.

The concept of a 2-step lap joint for the assembly of the sectionized blades as shown in Fig. 15(a) has been taken into interest for the determination of the stress and strain. The determination of the stress and strain at the surface of the lap-joint section of the assembly would predict the structural integrity of the assembled blades. Also, there can be another spot for the location of the strain gage at the outer step lap joint of the central blade assembled with another blade which can be considered an interest point of concern. To make safe installation of strain gage and safe prototype testing, the rectangular rosette strain gage is bonded closer to the inner lap-joint surface of the central blade of the test model. The strain gage now would determine the stress and strain for the inner lap-joint section under assembly with another blade during experimentation. The individual quarter bridge circuits are also patched closer region to the strain gage to avoid the degradation of the Analog signals. A hole of the size of 8mm is designed to be drilled on the surface of the blade closer to the lap joint section at an inclined angle so that all the wires of the bridge circuit are allowed to be passed down to the cavity of the hollow blade. Theoretically, the measurement system is capable of reading strain data from two rectangular rosette strain gages that can be bonded to the two VAWT blade models at any desired location of measurement during operation.

iii. Determination of the positioning of the ADCs.

All the ADCs connected to the bridge circuit of individual strain gages are designed to be kept inside the hollow cavity of the hollow VAWT blade. The size of ADC (25.3mm x 23.0 mm x 4.5mm) is fully able to be kept inside the hollow cavity of the blade (nuvoton, NAU7802 24-Bit Dual-Channel ADC For Bridge Sensors, 2012). Theoretically, each ADC is designed to be kept closer to the lap joint section near the hole of the blade. Each ADC is designed to be kept at a distance with minimum Analog wires consumed but also at an appropriate distance of 25cm from each other to avoid electrical interference.

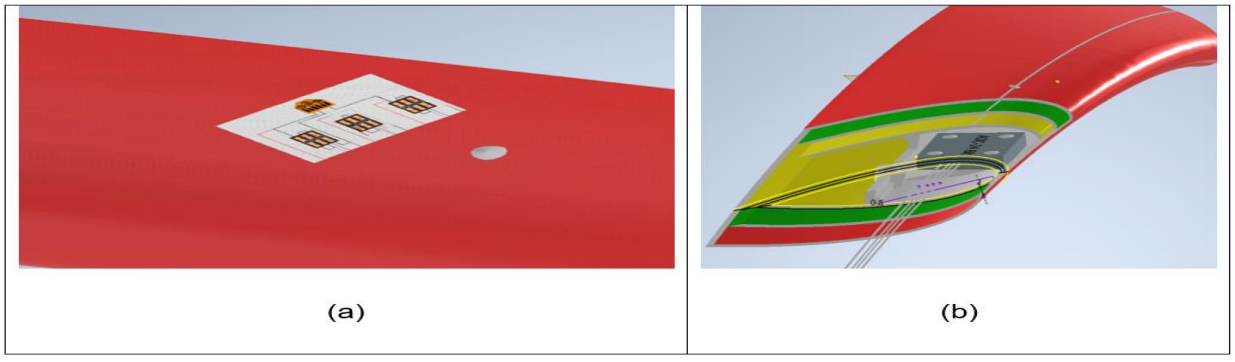

Figure 12: Positioning of Electronics; (a) Positioning of Strain gages and bridge circuit; (b) Positioning of ADC inside hollow cavity

iv. Design of Hollow cavity around the Spokes

For the design of the experimental measurement, the existing spokes of the VAWT model are to be modified to hollow spokes. The design of the spokes shouldn't affect the aerodynamic performance and the stability of the VAWT model. The hollow design of the spokes has been kept beyond the scope of the project. All the wires from ADCs of each strain gage are allowed to pass along the hollow cavity of the assembled blade to the top spokes. The hollow spokes would allow all the wires coming from the ADCs of each strain to gauge the shaft of the VAWT model.

v. Design of Electronics Holder

The positioning of the Multiplexer and ESP32, being the central data acquisition system and the point of the data transmission system, in such a rotatory system was another challenge to complete. The positioning of these electronics should be kept taking into consideration no/minimal impact on weight and aerodynamic performance in the VAWT model. The positioning of these electronics is designed to be kept inside the hollow shaft of the VAWT model. The size of the Multiplexer (2.15in.x1.40in.) and ESP32 (2.55in.x0.9in.) can be kept inside the hollow cavity of the shaft of the VAWT model having the 40mm of inner diameter with the design of the electronics holder. The designed electronics holder is capable of fitting inside the inner hollow cavity of the shaft. The design of the electronics holder is created in such a way the upper head of the spokes is attached to the upper surface of the spokes. There is an arrangement of two holes in a symmetry which allows the passage of the wires coming from the hollow cavity of spokes into the shaft and electronics holder. The electronics holder is connected to the shaft with the existing cross bolt in the VAWT model for which an exact hole size of 4mm is created to allow the cross bolt to penetrate the electronics holder.

Figure 13: Design of Electronics Holder

vi. Determination of the positioning of the MUX board, ESP32, and battery

The multiplexer and ESP32 model are connected to its base and fixed with a screw. The base of these electronics is allowed to pass down through the slots created in the internal hollow cavity of the holder. These electronics would be below the position of the cross-bolt connection. There is an arrangement for the positioning of the battery on the top surface of the electronics holder with the smaller profile of a rectangle (55 mm x 50 mm) slot for the battery.

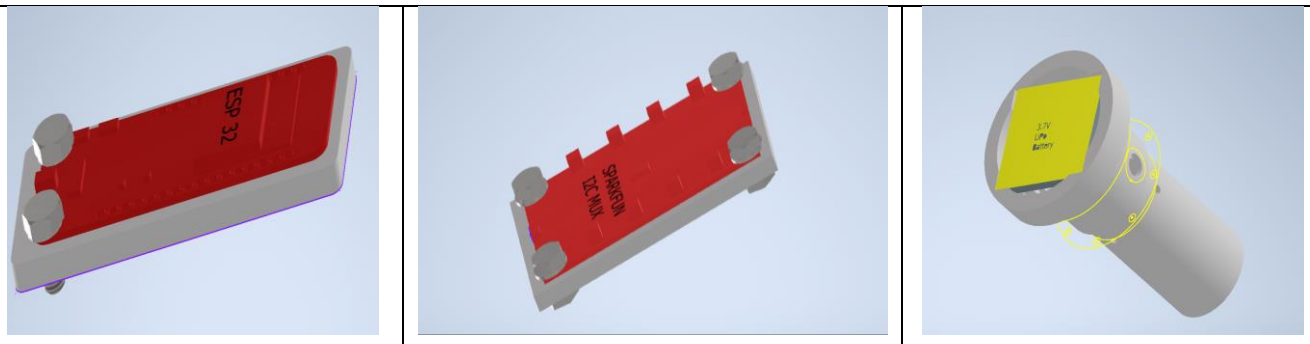

(a) (b) (c)

Figure 14: Positioning of Electronics in Holder; (a) ESP-32 fixed with base slot; (b) MUX board fixed with its base slot ; (c) Positioning of the battery in the holder

In this way, all the electronic components fit in the complex and compact geometry of the VAWT model without disturbing the aerodynamical performance of the model and the weight and force balance of the blade along the shaft-axis (See Appendix M).

3.6 Development of the Test Model

The test model is the assembly of the three recently designed VAWT blades with the feature of a hollow cavity supported by the Z-section along with the step-lap joint feature. The testing of the proposed measurement system on the test model focuses on the degree of performance over different small loading conditions and follows the theory to determine different forms of stresses and strains. Each of the following steps is explained in detail.

i. 3D printing of the new Hollow Blades.

The design of the recently developed VAWT blade includes three major attributes mainly, the hollow cavity throughout the helical profile of the blade, Z-section support along the curve for strength and support, and step lap-joint feature for the assembly of all blades. The 3D printing of the blade was carried out in ULTIMAKER 2+ which was available in the laboratories at Flinders University. The left end of the left blade and the right end of the right blade were modified to allow the end parts to be broad enough to provide enough strength and grip during clamping. The design layout of the end blades can be found in Appendix I.

ii. Creation of the Quarter Bridge Circuit

Wheatstone quarter bridge circuit is to be created for each of the strain gages of the rectangular rosette strain gage. Firstly, three thick surface mount 120 Ω resistors were soldered with strain gage connecting terminals TF-2SS and individually soldered as per the requirements of the bridge circuit. Special concern was given in determining the length of the QWICC wire coming from the quarter bridge circuit for the connection of ADCs to be placed at different separated distances along the hollow cavity of the VAWT blade. Special care was taken to the strain gauge while soldering the lead wires to the individual quarter bridge circuit. The soldering of the quarter bridge circuit was carried out as per the wiring diagram shown in Fig. 6.

iii. Soldering of the quarter bridge circuit, strain gauge, and ADCs.

Before the soldering of the circuit with ADCs, a borehole of 8mm in the upper surface of the blade was drilled to pass all the wires from the bridge circuit to the hollow cavity. The length of the QWICC wire was initially determined for individual ADCs to be positioned at the allocated space. The soldering of the 4 wires from the bridge to the ADC terminals was guided by the handbook of Adafruit NAU7802 24-bit ADC. The E^+ pad of the ADC was connected to the excitation voltage of the bridge with red wire. The E^-pad was connected to the ground with black color wire. The A^+ pad and A^- pad are connected to the differential output from the bridge configuration represented with white and brown wires.

iv. Installation of Strain Gage

The area of installation of the strain gauge is selected to the outer-surface region of the inner lap-joint of the central blade as this area is the region where two VAWT blades are glued and assembled. The positioning of the strain gauge at this region allows the study of the values of the stresses and strains generated on the surface of the lap joint and the integrity of the assembly.

Table 1: Installation of Strain Gage

S.N.	Steps	Activity
1.	Surface Preparation	Norton Saint-Gobain P1200 sanding sheet was used to create a very fine and clear surface around the position of the strain gauge.
2.	Fine Cleaning	The surface of the blade was cleaned using the isopropyl alcohol dipped with the cleaning tissue available in the laboratory.
3.	Tapping of the strain gage	The strain gauge was taken out from its sealed plastic sheet, picked up with the tweezers affecting the grid lines, and then stuck on the sticky tape for a while.
4.	Applying Adhesives	the cyanoacrylate adhesives as prescribed for the strain gage were dropped on the surface of the bonding area and spread out
5.	Curing and pressing	Manual pressing of the strain gauge was carried out for at least 2 minutes and then the force was applied with twisting and turning.
6.	Setting	The installed strain gauge was allowed to be set for a whole 24 hours so that the bonding strength could be perfectly established to full strength.

(Lab., 2021)

v. Positioning of all components and assembly of the Blades.

The sheets of the individual bridge circuit and all three blades were assembled with acrylic glue. Each ADC was positioned in its perfect position and double-tapped to attach firmly to the walls of the hollow cavity of the blades. Acrylic adhesives can maintain a fixture time of 10 minutes and 80% strength by 24 hours.

vi. Arduino Programming & Excel Live Data Streaming

The Arduino code was developed that allows the ESP32 microcontroller to receive the output values from each of the ADCs connected to strain gage bridge configurations from each of the channels of the Multiplexer as shown in APPENDIX K. The Excel Data Streamer function was deployed to ease the recording of Arduino output.

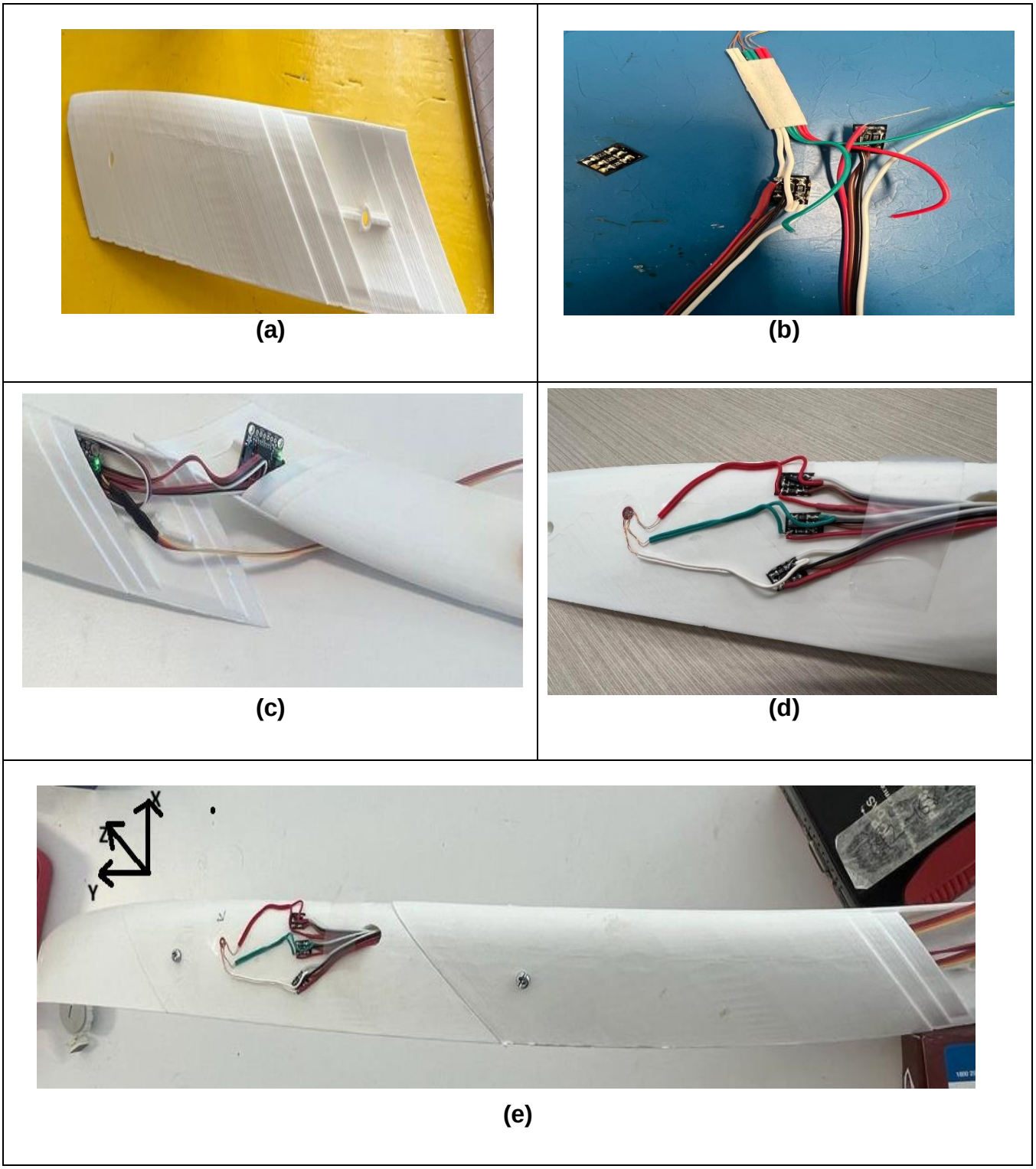

Figure 15: Development of Test Model: (a) 3D printing of blades; (b) Creation of Quarter Bridge Circuit;(c) Soldering of ADCs; (d) Installation of Strain Gage; (e) Developed Test Model

3.6 Experimental Testing and Validation by FEA Analysis

With the development of the test model, the experimentation and testing of the measurement system were carried out under static structural analysis. The experimental testing of the test model was carried out with 5 different loadings attached on the ends of the test model and fixed support at the lap-joint section opposite to the strain gauge. The digital strain values were obtained through Arduino programming and recorded in Excel. The values are then used to determine different forms of stresses and strains under different conditions mathematically.

The validation of the experimental results of stresses and strains was carried out with FEA analysis using ANSYS workbench software. The software can carry out to static structural analysis of the test model simulated under a similar environment as in the experiment with the material set as PLA and presents the values of required forms of stresses and strains under validation.

The approach of FEA analysis in ANSYS workbench is being guided by the following set of processes as presented below.

Figure 16: Processes of FEA Analysis

1. Geometric Modelling & CAD

The CAD files of the blades that were used in the development of the test model were assembled in Inventor software to represent the CAD model of the test specimen for FEA analysis. The unnecessary sketches and attributes in CAD assembly were omitted to create clean and proper faces and surfaces of the assembled model. The faces of the blades on both edges were slightly modified earlier during the development of the test model to distinguish the orientation of the position of strain gages and fixed support for ease in evaluation and analysis. The assembled CAD model is saved in.IGS format for compatibility with ANSYS workbench software.

2. Setting Material Properties

ANSYS workbench library is found to have limited material under the composite materials section in Engineering Data sources. Therefore, the physical, mechanical, and thermal properties of the Polylactic acid (PLA) were added to its library for analysis. The major properties of the material PLA like Density, Tensile strength, Yield strength, Young's modulus, shear

modulus, and Poisson's ratio. etc. were added to define the material properties of PLA. These values were carefully set to the same values that are also in experimental Testing.

3. Mesh Generation

The meshing of the test model was generated using the combination of the Mapped Face Meshing method and sweep meshing method to ensure capturing accurate structural behavior of the test model. Mapped Face Meshing was applied in the regular geometry areas whereas sweep meshing was targeted to areas of high concentrations like holes and areas around lap joints with the element size of 1mm.

4. Boundary & Loading Conditions

The model was provided with the fixed support in the right-sided lap joint of the central blade opposite to the thicker cross-section blade profile positioned on the left similar to the experimental test model. The application of the two vertical loads was carried out from the two side-wise holes on the edges directed vertically downwards. The values of the forces are changed to different experimental loads applied in the experiments sequentially.

5. Solver Setup

The solver was set to determine the results of maximum shear stress and stress intensity. The study of Shear Stress and Stress Intensity can be considered important in the sense that the experimental values of these parameters were based on the use of three principal strains, Young's modulus and Poisson's ratio applied which incorporates the major material characteristics. It can be considered appropriate for comparison and validation of results.

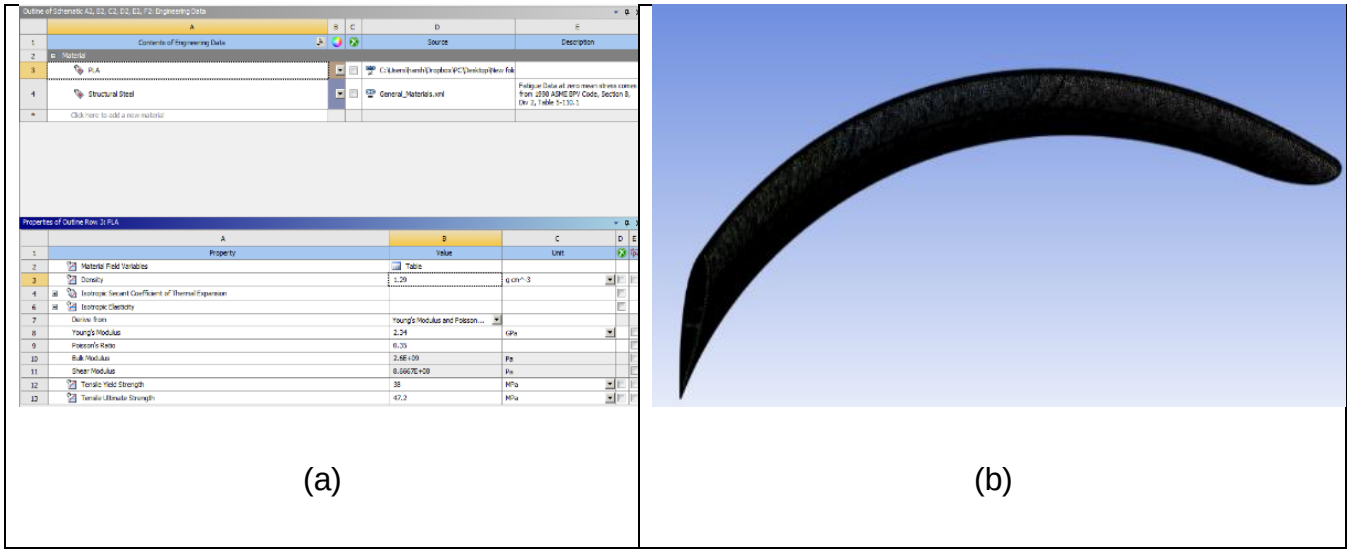

(a) (b)

Figure 17: FEA methods; (a) Defining Polylactic Acid material; (b) Mesh Generation

CHAPTER FOUR RESULTS AND DISCUSSION

4.1 Introduction

This chapter presents the outcomes from the experimentation of the designed measurement system installed in the test model subjected to static structural stress analysis. The chapter initiates with the output data of the experiments processed in Arduino programming software which was later data streamed to Excel for recording and presentation. Then the data is interpreted as the theory of conversions established in the methodology section to the point of determination of individual strain of each strain gauge. It includes the conversion of the change in digital values first to the differential voltage and then to the induced strain levels. These strain values are then interpreted with the formulas as per the principle of maximum stress and strain theory.

4.2 Results

4.2.1 Experimental Analysis

i. Experimentation

The developed test model with a rectangular rosette strain gauge under a quarter bridge circuit connected to individual Analog to Digital Convertor (ADCs) was connected to the ESP 32 module with the help of a MUX board and programmed in Arduino.

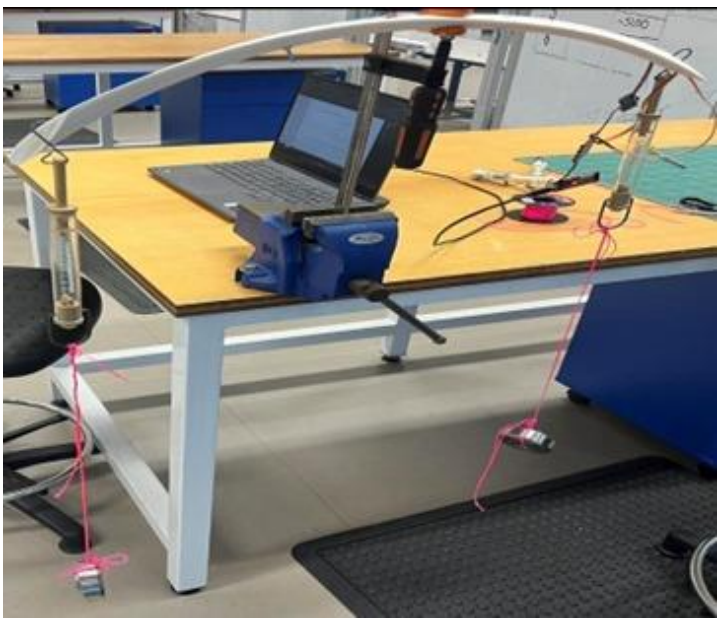

Figure 18: Experimental stress analysis

The static loading was carried out by providing fixed support in the right-side lap-joint section of the central blade opposite to the strain gauge and providing different loads on each end,

particularly at the end-hole section of the blade. The experimentation was carried out under 5 different loading conditions namely 3.5N, 8.5N, 10.5N, 12N, and 17N respectively with the help of available loads. The loads were hanged to the hole section using a spring balance as shown in the figure. (See in Appendix L)

ii. Data Acquisition

As discussed in the methodology, the whole data of the measurement system showing the digital value obtained from the Arduino code execution was data streamed to Excel providing the facility of recording the values as well as a live graphical representation of the loading. The representation of digital strain values before and after loading is represented by the following figure obtained on the experimentation of 8.5N loadings. The live recording of the data in the Excel data streamer was set to 150 milliseconds of data interval recording the values up to 500 rows with the newest data at the last row orientation. So, it means digital strain data from every strain gauge was recorded for every 150 milliseconds. These settings allow to show the graphical performance of the measurement system for 1 minute and 15 seconds of total time including before and after the loading stage. It represents an ample range of data of digital strains representing before-loading and after-loading stages which would be used for calculation of developed stress and strains in the region under loading.

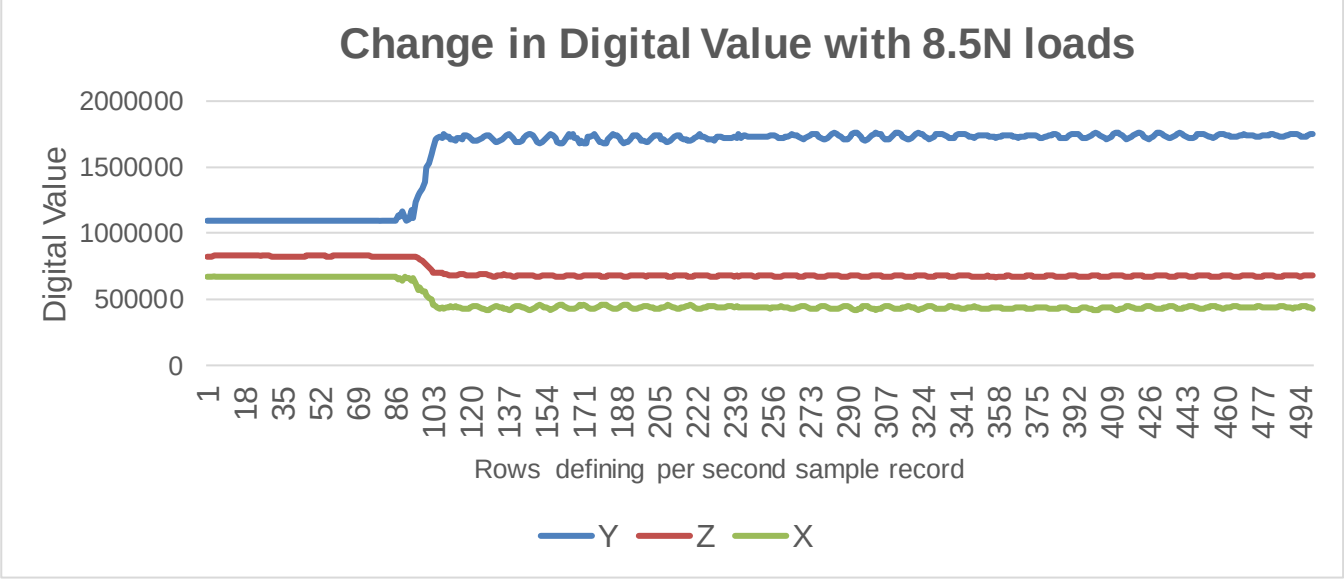

Figure 19: Change of Digital Strain Signals with 8.5N loading at each end

Figure 19 represents the nature of digital strain values during the experiment. The unloading stage of the test model is demonstrated by the straight lines of digital output values of each of the strain gages. With the application of the loadings of 8.5 N in each of the side-wise holes of the assembled blade, the strain gauge Y demonstrated a sharp rise in the value of the digital output signals. However, strain gage X and Z showed the nature of a sharp decrease in the value of the digital values. This sudden rise and fall in the digital values were caused by the

introduction of the loadings at each end. Therefore, the change in the digital values for each of the strain gages should be the measure of the stress and strain generated in the 3 different directions as the strain gages are oriented. To explain the nature of one strain gage Y showing the rise and the other two showing the fall, it can be addressed by the mis-soldering of the higher potential point of the Wheatstone bridge circuit to A^- pad of ADC and similarly lower potential point of Wheatstone bridge connected to A^+ pad of ADC in the wiring of Strain gage X and Z. However, the major concern should be on the change of the output value of the digital signals rather than rise and fall. All these strains and stress measured by the strain gauge fall upon the tension forces acting on the upper surfaces of the test model subjected to bending forces. With the application of the loading, the surfaces are allowed to be stretched representing tension. The directionality of the strains and stresses have been marked as X, Y, and Z axes as shown in Fig.15 (e)

Table 2: Statistical Analysis of the Experimental Data for 8.5N loading.

	Before Loading Stage			After Loading Stage		
Parameters	Y	Z	X	Y'	Z'	X'
Average	1096303	827365.6	671922.8	1725342	679073.5	438854.5
Standard Deviation	1275.816	641.3693	1083.725	41448.63	12027.77	15629.72
Coefficient of Variance	0.116374%	0.077519%	0.161287%	2.402343%	1.771203%	3.56148%

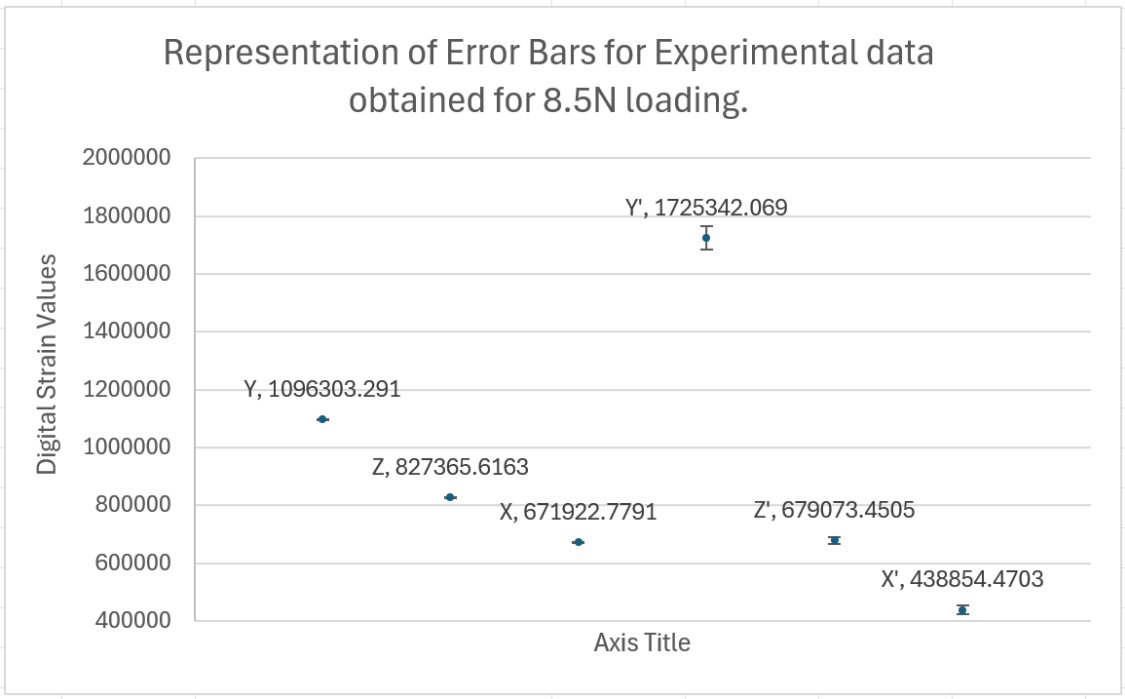

Figure 20: Representation of Error bars in the Experimental Data.

Fig. 20 represents the variation of the experimental data concerning the average value of digital strain values before and after loading stages. During the before-loading stage, the digital strain signals seem to be almost constant throughout the period with lesser standard deviation and

coefficient of variation. With the application of the loading, the digital values are found to be fluctuating but the standard deviation of the experimental data shown in the form of error bars provides evidence that the experimental data are majorly close to the average digital values. The standard deviation can be seen as a bit large in Y-strain data and other strains are heavily concentrated around the average digital values. Therefore, average digital values can be the best reference point to represent all the experimental data for both stages.

Similar experimentation was carried out following the same procedure with different specified loads on the ends of the test specimen with the same constraints.

iii. Data Interpretation

The interpretation of the change of digital output value to the differential voltage generated and then to strain-induced is to be performed.

As mentioned in the theory involved, eqn. (1) provides relation

$Voltage\ value = \frac{\Delta Digital\ values}{2^n - 1} * \frac{V_{ref}}{Gain}$ (SparkFun, n.d.)

For voltage-to-strain conversion; $V_0 = \frac{VEX}{4} * K * \in$ i.e. $\in = \frac{4}{VEX * k} * V0$

Table 3: Conversion of Average Digital Value (ADV) to Strains for loading of 8.5N at both ends.

Strain Gage	ADV before loading	ADV after loading	Change in ADV	Voltage Output	Strain-induced
X-Strain Gage	671923	438854	233069	0.520mV	$\in_1$=336.56 μ$\in$
Y-Strain Gage	1096303	1725342	629039	1.406mV	$\in_2$=910.03μ$\in$
Z-Strain Gage	827366	679073	178293	0.398mV	$\in_3$=257.60μ$\in$

We have given parameters, $\in_1$== 346.278 μ$\in$; $\in_2$= 954.69 μ$\in$; $\in_3$=219.417 μ$\in$; E= 2.34 GPa for PLA; ν= 0.35 for PLA ((Data, n.d.) (See in Appendix F)

Table 4: Calculation of Stresses and strains for 8.5N loading.

Parameters	Formula	Calculated Value
Maximum Principal Strain (ϵ_{max})	$\frac{1}{2}\left[\epsilon_1+\epsilon_2+\sqrt{2*\{(\epsilon_1-\epsilon_3)^2+(\epsilon_2-\epsilon_3)^2\}}\right.$	**1087.99 μ∈**
Minimum Principal Strain (ϵ_{min})	$\frac{1}{2}\left[\epsilon_1+\epsilon_2-\sqrt{2*\{(\epsilon_1-\epsilon_3)^2+(\epsilon_2-\epsilon_3)^2\}}\right.$	**158.591 μ∈**
Maximum Shearing Strain (γ_{max})	$\sqrt{2*\{(\epsilon_1-\epsilon_3)^2+(\epsilon_2-\epsilon_3)^2\}}$	**929.407 μ∈**
Maximum Principal Stress (σ_{max})	$\frac{E}{1-\nu^2}(\epsilon_{max}+\nu\,\epsilon_{min})$	**3.049MPa**
Minimum Principal Stress (σ_{min})	$\frac{E}{1-\nu^2}(\epsilon_{min}+\nu\,\epsilon_{max})$	**1.438MPa**
Maximum Shearing Stress (ζ_{max})	$\frac{E}{2(1+\nu)}\gamma_{max}$	**0.805MPa**
Stress Intensity	$\frac{E}{(1+\nu)}\gamma_{max}$	**1.610MPa**

With this method of the calculation shown above, similar graphs and experimental calculations were carried out for the remaining loadings conditions i.e. 3.5N, 10.5N, 12N, and 17N. The loading conditions, fixed support, and all other programming setups were kept constant for every experimentation. All the calculations for each loading experiment are shown in Appendix N.

iv. Calibration of the Strain Gage Sensor

The approach of the calibration of the strain gauge sensor used for the assembly of three 3D printed VAWT blades involves the combination of the experimental stress analysis and successive validation by FEA analysis. During experimental stress analysis, while in the before-loading stage, a stable digital strain level was maintained compensating for the electronic and mechanical drift produced during experimentation. Standard Measured weights were applied on both edges and a stable digital strain level was recorded for proper experimentation avoiding

unnecessary vibrations and fluctuations. The experimentation was carried out at normal room temperature to avoid the account of temperature compensation caused by rise/fall of temperature. The deformation and change in digital strain values were recorded in Excel for proper evaluation and interpretation of the experimental data. Multiple attempts for each loading condition were carried out to ensure the repeatability and reproducibility of similar results under similar environments. Then the FEA analysis was carried out for each of the experiments. Similar environments, material properties, boundaries, and loading conditions were deployed for the simulation of the test model for static structural stress analysis. The omission of the unnecessary sketches and surfaces along the CAD model and improvements in meshing conditions were applied to ensure the simulated results present better cohesion to the experimental results. Finally, the comparison and validation of the experimental results and FEA results were carried out to evaluate the performance.

4.2.2 FEA Analysis

The FEA analysis was carried out as per the preparation described in the methodology section. FEA analysis for the validation of each experimental result was carried out with the respective values of loading and boundary conditions with the material defined as Polylactic acid (PLA). The major result parameters set for the comparison and validation were the maximum shear stress and stress intensity. The values of the experimental data were validated with the FEA results probing the position of a strain gauge in the simulated model as presented in the figure below.

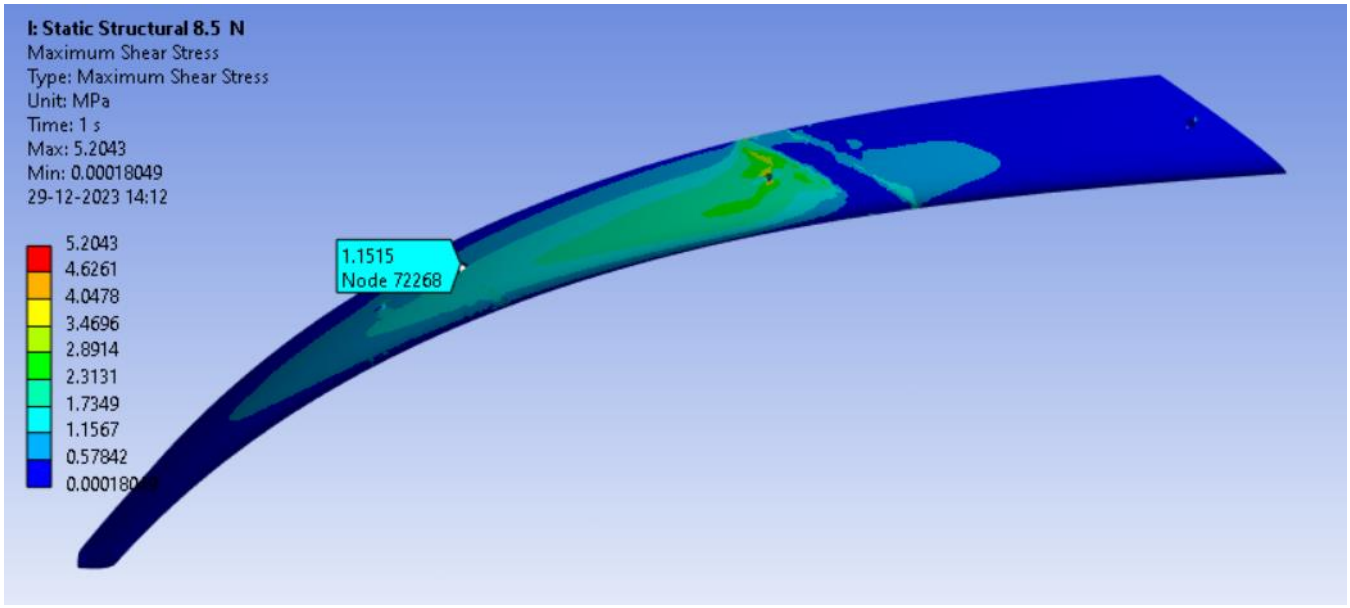

Figure 21: Maximum Shear Stress at the position of strain gage for 8.5N at end holes of assembly

Fig. 21 shows the value of the maximum shear stress probed to the region of the strain gauge. This position represents the region of the outer surface of the inner lap-joint section of the central

blade assembled with the left-sided blade in the test model. The FEA analysis shows the maximum value of shear stress in the region near the fixed support i.e., the lap-joint section of the central blade opposite to the strain gauge. However, the stress analysis of the area where the strain gauge is bonded is very crucial because it provides information on the stresses and strain values developed under such loading conditions at the area where two blades are assembled. These areas of the lap joint are the region where the entire integrity of the VAWT blade assembly is based.

4.2.3 Validation of Experimental Stress Analysis with FEA Analysis under Different Loading Conditions.

The validation of the experimental stresses obtained from the strain gauge measurement system was carried out with the determination of the stresses from the FEA Analysis. The major parameters were considered for the comparison namely maximum shearing stress and stress intensity. The values of these parameters were obtained using the probe feature in ANSYS to the area of the position of the strain gauge. Then the values of each of the parameters were compared and analysed for validation in Excel.

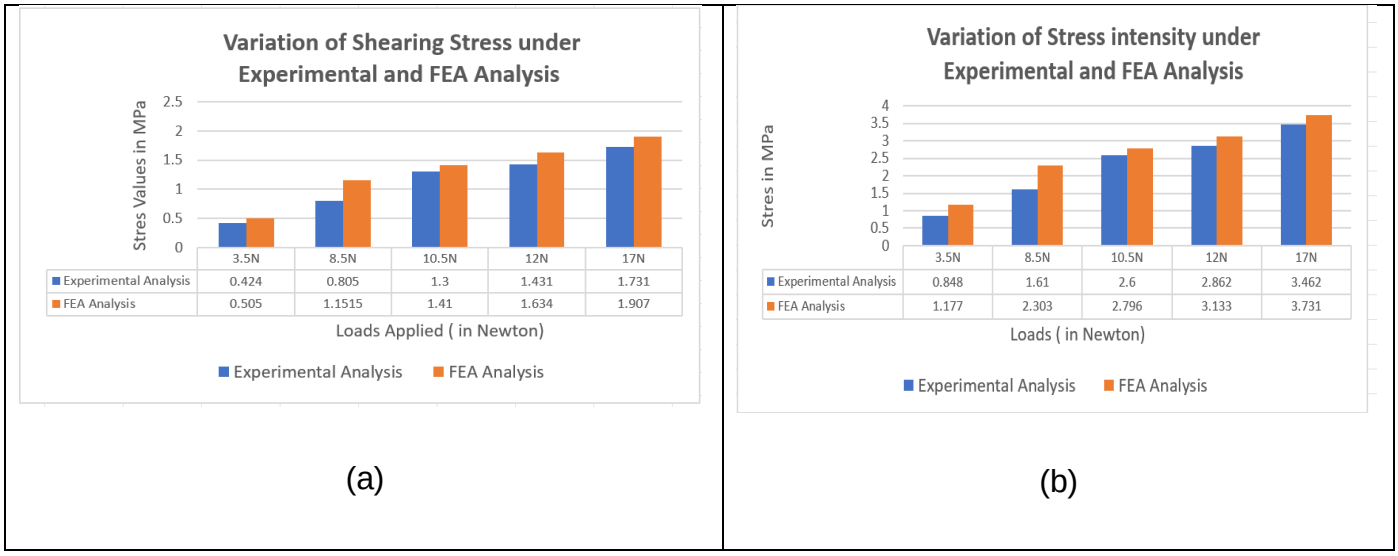

Figure 22: Validation of Experimental & FEA results; (a) Variation of Shearing Stress; (b) Variation of Stress Intensity

Figure 22 shows the variation between the experimental and FEA results. The nature of the experimental maximum shearing stress and stress intensity are much closer to the values obtained in the FEA analysis. It was observed that both analyses showed a linear trend of progression. The values of stresses were found to be gradually increasing with the increase in the loads. However, the overall trend of progression is much more like each other. The results of the FEA analysis for the Maximum shearing stress and stress intensity were found to be higher than the experimental analysis. The difference in the values of each parameter for a particular load under experimental and FEA analysis is found to be under 10-12%. It can be

concluded that the values were satisfactorily closer to each other following a similar trend of progression.

4.3 Discussion

The experimental stresses obtained during the testing are under the theories of stress and strains. As the research done by P.Sadanandam, Reddy, & Timmapuram, (2021) under the application of the vertical loads in a blade specimen, bending forces are developed which generates tensile stress on the upper surface of the blades having materials being stretched. As per the literature where blades are normally tested in the cantilever position, the test model has been tested with two vertical loads at the ends with fixed support in the middle. The results provide evidence of tensile stress generated on the surface in all 0,45 and 90 orientations. The results also provide the evidence that highest tensile stresses are developed in the designated Y-axis than other orientations due to the impact of vertical loads which adhere to the basic principles of mechanics.

The experimental stress obtained from the testing is in complete adherence to the theories of conversion of digital values to voltage using ADC, voltage to strain conversion for quarter bridge circuit, and relation of strains to different forms of stress and strain by theories of Maximum principal stress and strain. As per the article published by Spark Fun,(n.d), the conversion of the digital values to voltage values is dependent on the four major parameters namely change in digital values obtained, referencer voltage of the system, resolution of the ADC, and gain of the ADC. The article published by Bestech,(n.d.) relates that the change in voltage value in wheat-stone bridge to the generated strain in the strain gauge is dependent on the excitation voltage and gage factor of the strain gauge. The experimental stress obtained from the testing is in complete agreement with these theories to determine the further stress parameters like principal stress and strains, shearing stress and strains using the theories of Maximum principal stress and strains.

As per the paper published by Anderson Langone, et al. (2018), strain gage is connected to a Wheatstone bridge configuration having Nano shield Loadcell to facilitate the connection and Arduino Mega2560 as the micro-controller. The system is facilitated with an amplifier, a filter, and a 20-bit ADC for signal conditioning. The paper suggested the use of this method to have good efficacy in applications with satisfactory accuracy. The project has also applied a similar approach to obtain the project objectives under the system requirements and stakeholders' requirements for the VAWT model. However, the project carried out experimentation with fixed support in between two vertical loads at the ends of the test specimen rather than the cantilever position due to the curved and very long profile of the test specimen. The use of the 24-bit ADC

and ESP-32 module facilitated the concept of wireless transmission of the data in the case of the VAWT model.

One of the major limitations of the project was the correction of any errors caused by small variations in the resistance of a resistor in the Wheat-stone bridge circuit leading to unbalancing of the bridge. The project considered the use of ±1% tolerance limit of 120 Ω would have negligible error in balancing the Wheatstone bridge. The offset in bridge completion was also justified with the reasoning of taking the change in digital values as a measure starting point for the determination of stress and strain. Whatever the voltage value of the strain digital value at the before-loading condition may be present, the rise or fall of the voltage values depicted by the change in digital data would be used for the determination of stress and strain by that loading. One of the major future improvements in the measurement system developed in the project would be the balancing of the Wheatstone Bridge using the potentiometer. With the development of the test model, it can be advised all the patches of the quarter bridge circuit used for the strain gauge could be kept inside of the hollow blade initially so that the aerodynamic performance of the VAWT blades would be less affected.

The difference in the experimental results and simulated results can described due to the influence of various factors. The results obtained from the experimental analysis are solely dependent on the nature, strength, density, and other material properties of the specific test model prepared using 3D printing technology. The actual values of the strength, density, and other material properties like Young's modulus, Poisson ratio, ultimate tensile strength, etc. are dependent upon how the model has been manufactured during 3D printing, its infill density, cooling temperature, and other methods. The experimental analysis projects the stress and strain with the actual properties of the blade and the model. However, the simulation of the test model utilizes the material properties generated from the literature reviews for PLA material which may not be the actual values of the printed materials. The simulation results are also impacted by the meshing conditions developed in the test model and the nature of boundary conditions. However, the experimental and theoretical values have been satisfactorily closer to each other thereby validating the experimental results.

CHAPTER FIVE CONCLUSION AND FUTURE WORKS

Conclusion

The project is solely focused on the design and development of the stress-strain measurement system that can be applied to the existing Vertical Axis Wind turbine (VAWT) blades. With the study of various literature reviews on different existing stress & strain measurement systems, types of data acquisitions, and interpretation methods for wind turbine blades, the project is carried out with the application of strain gages having a quarter bridge circuit connected to the set of data acquisition system developed using 24-bit Analog to digital converter, multiplexer, and ESP32 as micro-controller for the wireless transmission of the data in the rotatory VAWT model. This is one of the innovative approaches identified for stress measurement systems applicable to the VAWT model. The project identifies the mechanical and electrical layout for the positioning and integration of the measurement system within the VAWT model. The test model for the testing of the performance of the developed stress-strain measurement system is composed of an assembly of 3 sectionized hollow blades which provides evidence of how the system is fit in the existing model. The static stress analysis of the test model under different loading conditions demonstrates the sensitivity of the measurement system to minor loadings. The project has been capable of introducing a stress and strain measurement system to fit inside the compact geometry of the VAWT blades and the system itself. The project provides a simple and cost-efficient method that can be installed in the VAWT model. The project has successfully presented the method of experimental determination of stresses and strains using strain gages along with ADCs and micro-controllers like ESP-32 under the Arduino IDE platform. The experimental results and FEA results are found to be satisfactorily close to each other.

Future Works

Firstly, the Balancing of the Wheatstone bridge circuit for each strain gauge could be carried out to enhance the precision of the measurement system. It can be carried out with the help of a potentiometer to determine and omit the initial voltage offset in the bridge. Secondly, the patch of quarter bridge circuits developed for each strain gage could be kept inside the hollow blade by the 3D printing of the top and bottom surface of the blade separately and then gluing them together. It would greatly reduce any aerodynamic impact caused by the bridge circuits patched on the surface of the blade. Thirdly, the developed stress and strain measurement system can also be operated by the power sources stationary in the ground connected through the slip rings mechanism along the shaft which would omit the use of a separate battery used for the project.

BIBLIOGRAPHY

Dally , J., & Sanford , R. (1987). Strain-Gage Methods for Measuring the Opening-Mode Stress-Intensity Factor, K,.

Anderson Langone, S., Marcus, V., Arthur, Mereles, G., Clivaldo, O., & José, M. B. (2018). A study of strain and deformation measurement using the Arduino microcontroller and strain gauges devices.

Bechly, M., & Clausen, P. (1995). Structural design of a composite wind turbine blade using finite element analysis. *Structural design of a composite wind turbine blade using finite element analysis*.

Bestech. (n.d.). *UNDERSTANDING A WHEATSTONE BRIDGE STRAIN GAUGE CIRCUIT*. Retrieved from UNDERSTANDING A WHEATSTONE BRIDGE STRAIN GAUGE CIRCUIT: https://www.bestech.com.au/blogs/understanding-a-wheatstone-bridge-strain-gauge-circuit/

Brand, M. M.-A. (n.d.). *Stress Analysis-Strain Gages (Gauges)*. Retrieved from Micro Measurments-A VPG Brand: https://micro-measurements.com/stress-analysis-strain-gages

Carr, J., Baqersad, J., Niezrecki, ,., Avitabile, P., & Slattery, M. (2012). Dynamic Stress–Strain on Turbine Blades Using Digital Image Correlation Techniques Part 2: Dynamic Measurements.

components, R. (n.d.). *Yageo 120Ω, 1206 (3216M) Thick Film Resistor ±1% 0.25W - AC1206FR-07120RL*. Retrieved from RS components: https://au.rs-online.com/web/p/surface-mount-resistors/1978255?redirect-relevancy-data=7365617263685F636173636164655F6F726465723D31267365617263685F696E746572666163655F6E616D653D4931384E525353746F636B4E756D62657226736561726368 5F6D617463685F6D6F64653D6D6174

Data, M. M. (n.d.). *Overview of materials for Polylactic Acid (PLA) Biopolymer*. Retrieved from MatWeb Material Property Data.

Energy, V.-X. (n.d.). *Advanced Vertical Axis Wind Turbines*. Retrieved from Advanced Vertical Axis Wind Turbines.

Fernández, L. (2023). *Share of wind electricity generation worldwide 2010-2022*. Retrieved from Share of electricity generation from wind energy sources worldwide from 2010 to 2022.

Hoffmann, K. (1987). An Introduction to Measurements Using Strain Gages.

Instruments, T. (2019). *TCA9548ALow-Voltage8-ChannelI2CSwitchwithReset.*

lab, T. M. (2021). *Foil Strain Gauges Fseries (GOBLET) .*

Lab., T. M. (2021). *TML Strain Gauges 2021 Precise & Flexible.* Tokyo Measurements Instruments Lab.

Li, Q., Maeda, T., Kamada, Y., Murata , J., Furukawa, K., & Yamamota, M. (2015). Effect of number of blades on aerodynamic forces on a straight-bladed Vertical Axis Wind Turbine.

Li, Q., Maeda, T., Kamada, Y., Muratab, J., Furukawa, K., & Yamamoto, M. (2015). Effect of number of blades on aerodynamic forces on a straight-bladed Vertical Axis Wind Turbine.

Measurements, M. (n.d.). *Rectangular Rosette Pattern Strain Gages*. Retrieved from Rectangular Rosette Pattern Strain Gages: https://micro-measurements.com/rectangular-rosette-patterns

Micro Measurements-a VPG Brand . (2020). *Strain Gage Sensor Reference Guide.* Retrieved from Micro Measurements: https://docs.micro-measurements.com/?id=8690

nuvoton. (2012). *NAU7802 24-Bit Dual-Channel ADC For Bridge Sensors.*

nuvoton. (2012). *NAU7802 24-bit Dual-Channel ADC For Bridge Sensors .*

P.Sadanandam, Reddy, P., & Timmapuram, V. S. (2021). Stress Distribution on Turbine Blade along with Root at Several Operating Speeds . *Stress Distribution on Turbine Blade along with Root at Several Operating Speeds* .

Pérez, J. S., Torres-Arredondo, M. A., & Güemes, A. (2015). Damage and nonlinearities detection in wind turbine blades based on strain field pattern recognition. FBGs, OBR and strain gauges comparison.

Qing'an, L., Takao, M., Yasunari, K., Junsuke, M., & Kazuma, F. (2015). Effect of number of blades on aerodynamic forces on a straight-bladed Vertical Axis Wind Turbine . *Effect of number of blades on aerodynamic forces on a straight-bladed Vertical Axis Wind Turbine* .

SparkFun. (n.d.). *Analog to Digital Conversion*. Retrieved from SparkFun Electronics : https://learn.sparkfun.com/tutorials/analog-to-digital-conversion/all

Systems, E. (2023). *ESP32 WROOM 32E.*

Thomsen, K., & Sorensen, P. (1999). Fatigue loads for wind turbines operating in wakes.

TML. (n.d.). *Connecting Terminals*. Retrieved from TML : https://tml.jp/e/product/strain_gauge/tansi_list.html

Yu, Z.-Y., Zhu, S.-P., Liu, Q., & Liu, Y. (2017). A New Energy-Critical Plane Damage Parameter for Multiaxial Fatigue Life Prediction of Turbine Blades. *A New Energy-Critical Plane Damage Parameter for Multiaxial Fatigue Life Prediction of Turbine Blades*.

Zhanwei, L., Binrong, W., Zhike, P., Xingjian, D., & Yegao, Q. (2019). Dynamic modeling and analysis of wind turbine drivetrain considering the effects of non-torque loads . *Dynamic modeling and analysis of wind turbine drivetrain considering the effects of non-torque loads* .

APPENDICES

APPENDIX A: Decision Matrix for the Selection of the Appropriate Stress & Strain Measurement System.

Table 5: Decision Matrix for different stress-strain measurement systems

Decision Criteria	**Weight**	**Strain Gage**	**Fiber Optic Sensor**	**Digital Image Correlation**	**Acoustic Emission Sensor**
Accuracy	0.2	High	High	High	Medium
Reliability	0.2	High	Medium	High	Medium
Durability	0.2	Medium	Medium	Medium	Medium
Sensitivity	0.15	High	Medium	High	low
Low Cost	0.15	High	Low	Low	Medium
Ease of Installation	0.1	High	High	Medium	Medium
		Selected			

Appendix B: Properties of ‘FRAB-1-11-1LJB-F’ rectangular rosette strain Gage

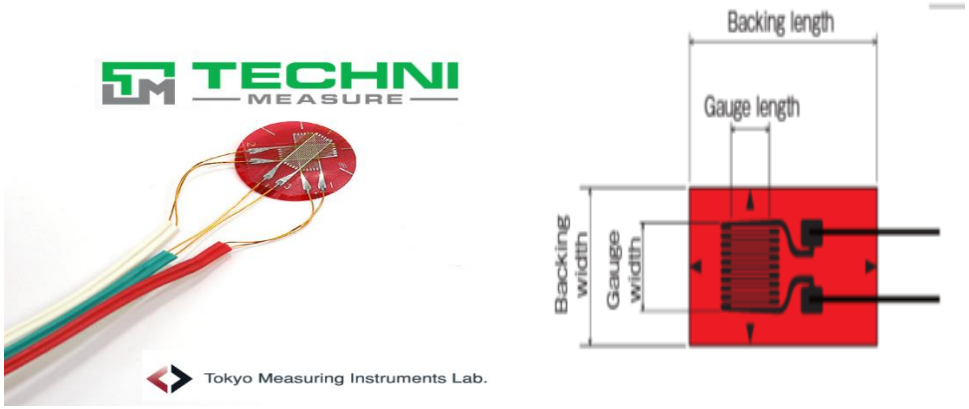

Figure 23: FRAB-1-11-1LJB-F

Table 6:Specification of 'FRAB-1-11-1LJB-F' rectangular rosette strain gage

S.N.	Properties	Specifications
1.	Gauge Length	1mm
2.	Gauge Width	0.7mm
3.	Backing length	Φ4.5
4.	Backing Width	Φ4.5
5.	Gauge Resistance	120±0.5 Ω
6.	Gauge Factor	2.06 ±1% for each
7.	Temperature Compensation	11*10^-6 /°C
8.	Lead-wires	0.44Ω/m

(Lab., 2021)

Table 7: Specifications of Thick Film Resistor

Resistance	Technology	Package	Tolerance	Power rating	Automotive Standard
120 Ω	Thick Film	1206(3216M)	±1%	0.25W	AEC-Q200

(components, n.d.)

Table 8: Specification of Strain Gage Connecting Terminals TF-2SS.

Type	Dimensions (mm)	Temperature range (°C)	Use
TF-2SS	4.6 3.8*0.2	-196 to 180 °C	Foil shape for general use.

(TML, n.d.)

Appendix C: Strain Gage Connecting Terminals and surface mount resistor used

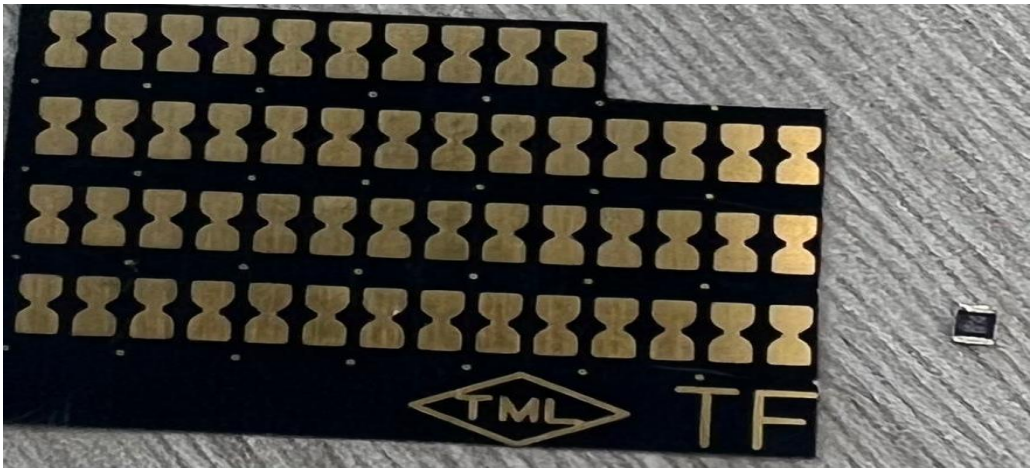

Figure 24: Strain Gage Connecting Terminals and surface mount resistor used.

APPENDIX D: Power Calculation for selection of battery

Table 9: Power Calculation for Battery Selection

S.N.	Component	Operating Voltage	Operating Current	Power Consumed
1.	ESP32	2.3V-3.6V	80mA	0.288W
2.	MUX board	1.6V-5.5V	20mA	0.066W
3.	ADC	3.3V	2mA	0.006W @ 6ADCs =0.0396W
4.	Strain Gage	3.0V (excitation Voltage with 120)		0.075W@ 6 strain gage = 0.45W
	Total Power Consumed			0.8436W
	For commercial V= 3.7V		For P=IV, 0.8436= I*3.7 **I= 0.228A**	

(nuvoton, NAU7802 24-bit Dual-Channel ADC For Bridge Sensors , 2012); (Instruments, 2019); (Systems, 2023)

APPENDIX E Conversion of Differential Voltage in the bridge configuration to the strain values.

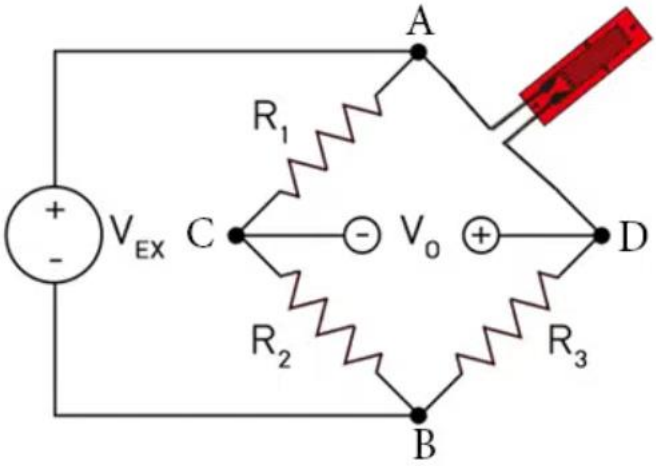

Let us consider the quarter bridge circuit shown in the figure above. Let R_1, R_2, and R_3 be the fixed resistor and R_4 be the resistance of the strain gauge. On loading and deformation, let the change in the resistance be ΔR.

Now, using the voltage divider rule,

The voltage at the point C = $\frac{R1}{R1+R2}V_{EX}$ (Bestech, n.d.)

The voltage at the point D=$\frac{R4+\Delta R}{R4+\Delta R+R3}$ * V_{EX}

Now,

$V_0 = \frac{R4+\Delta R}{R4+\Delta R+R3} * V_{EX} - \frac{R1}{R1+R2} * V_{EX}$

For $R_1=R_2= R_3 = R_4 = R$,

$V_0 = \frac{VEX * \Delta R}{4R+2\Delta R}$

Now, since R>> ΔR and 4R>>2 ΔR;

We get,

$V_0 = \frac{VEX}{4} * \frac{\Delta R}{R}$

Now, in the above equation, ΔR/R is the electrical strain, and the gauge factor is termed as the ratio of the electrical strain and the mechanical strain. Therefore, the above equation can be re-written as:

$V_0 = \frac{VEX}{4} * K * \in$ (Bestech, n.d.) eqn (2)

Which is the relationship between differential voltage with the mechanical strain where,

VEX (excitation voltage) = 3.0V ;

Gage Resistance (K)= 2.06 ;

APPENDIX F: Use of Maximum Principal Stress & Strain Theories;

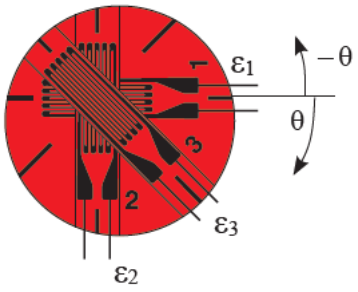

1st axis : ε_1
2nd axis : ε_2 at 90° position
3rd axis : ε_3 at 45° position

(Lab., 2021)

With the conversion of every voltage into mechanical strain, the values of mechanical strains $\epsilon_1, \epsilon_2, \epsilon_3$ can be determined which represents each of the strain gage of the rectangular rosette strain gage as per the direction of each of the strain gage shown in the picture above.

With these three values, the theories of Maximum principal stress and strains can be deployed to obtain each of the values of theoretical strains and stress.

i. Maximum Principal Strain: $\epsilon_{max} = \frac{1}{2}\left[\epsilon_1+\epsilon_2+\sqrt{2*\{(\epsilon_1-\epsilon_3)^2+(\epsilon_2-\epsilon_3)^2\}}\right.$

ii. Minimum Principal Strain: $\epsilon_{min} = \frac{1}{2}\left[\epsilon_1+\epsilon_2-\sqrt{2*\{(\epsilon_1-\epsilon_3)^2+(\epsilon_2-\epsilon_3)^2\}}\right.$

iii. Maximum Shearing Strain : $\gamma_{max} = \sqrt{2*\{(\epsilon_1-\epsilon_3)^2+(\epsilon_2-\epsilon_3)^2\}}$

iv. The angle from ε1 gauge to the direction of principal strain: $\theta = \frac{1}{2}\, tan^{-1}\{\frac{2\epsilon_3-(\epsilon_1+\epsilon_2)}{\epsilon_1-\epsilon_2}\}$

If ε1>ε2, the angle to the maximum principal strain is rotated by θ clockwise from the 1st axis, and the minimum principal strain is located at θ+90°. If ε1<ε2, the angle to the maximum principal strain is rotated by θ+90° clockwise from the 1st axis, and the minimum principal strain is located at θ.

Similarly, the values of stresses can also be calculated in terms of maximum principal stress and minimum principal stress which can be listed below :

Maximum Principal Stress $\sigma_{max} = \frac{E}{1-\nu^2}\,(\,\epsilon_{max}+\nu\,\epsilon_{min})$

Minimum Principal Stress $\sigma_{min} = \frac{E}{1-\nu^2}\,(\,\epsilon_{min}+\nu\,\epsilon_{max})$

Maximum Shearing Stress $\zeta_{max} = \frac{E}{2(1+\nu)}\,\gamma_{max}$ (Lab., 2021)

E Young's Modulus of Elasticity 2.34 GPa.

Poisson's ratio (ν) = 0.35 for PLA. ((Data, n.d.)

APPENDIX G: List of procurements

College of Science & Engineering

Requisition for Purchase

	Area	Ext No.	Buyer's Initials	Purchase Reference
023 /	CSE	/	/	/

DELIVER TO: FLINDERS UNIVERSITY, SCIENCE & ENGINEERING STORE, PHYSICAL SCIENCES ROAD, BEDFORD PARK, SA 5042
EMAIL TO: cse.store@flinders.edu.au

REQUESTOR DETAILS		SUPPLIER DETAILS	
Deepak Sapkota		**NAME:** Bestech Sensors & Teaching Equipment	
PHONE NO: 0406566801		**ADDRESS:** Unit 14, 44 Garden Bvd, Dingley VIC 3172.	
OR: Dr. Amir Zanj		**CONTACT:** 03 9540 5100	**WEB:** https://www.bestech.com.au/
sapk0063@flinders.edu.au		**PHONE NO:** 03 9540 5100	**EMAIL:** pehrlich@bestech.com.au

Y	PART/CAT. NO.	DESCRIPTION	UNIT PRICE EX. GST	TOTAL COST EX. GST	ENTITY	COST CENTRE XXX	PROJECT XXXXX	EXPENSE CODE XXXX
	KFPE-2206231	GFRAB-3-70-5LJCT 1. 3-element strain gage 2. Gage Length : 3mm 3. Gage Resistance: 120 ohm 4. 5M 0.11mm2 3-wired paralleled vinyl lead wires 5. Compensation material : All kinds of Plastics, ABS, polystryene, polycarbonate, polyacetal	$ 752	$ 752	01			
			TOTAL: $ 752					

The part No. mentioned is the quote reference provided to me during the quotation.

DO YOU REQUIRE QUOTES? *Please attach*		
VALUE	**QUOTATIONS REQUIRED**	
	Single oral or written quote	☐
: $10,000	Two oral or written quotes	☐
< $15,000	Two written quotes	☐
< $100,000	Three written quotes	☐
)	Tender or RFP unless otherwise exempted	

PURCHASE AUTHORISATION

I authorise payment of this purchase(s) against the account(s) as detailed above, and acknowledge my responsibilities in ensuring that the purchase is being made in accordance with:

1) Flinders University Financial Services Policies and Procedures** http://www.flinders.edu.au/finance/

2) Flinders University Work Health and Safety Policies and Procedures for risk assessment* prior to the purchase of hazardous chemicals and plant http://www.flinders.edu.au/whs/

NAME:

SIGN:

Flinders UNIVERSITY
College of Science & Engineering

College Store

Requisition for Purchase

Date	Area	Ext No.	Buyer's Initials	Purchase Reference
31/07/2023 /	CSE	/	/	/

DELIVER TO: FLINDERS UNIVERSITY, SCIENCE & ENGINEERING STORE, PHYSICAL SCIENCES ROAD, BEDFORD PARK, SA 5042
EMAIL TO: cse.store@flinders.edu.au

REQUESTOR DETAILS		SUPPLIER DETAILS	
NAME: Deepak Sapkota		**NAME:** Core Electronics	
ROOM NO:	**PHONE NO:** 0406566801	**ADDRESS:** 18/132 Garden Grove Parade, Adamstown NSW 2289, Australia	
SUPERVISOR: Dr. Amir Zanj		**CONTACT:** (02) 4058 2818	**WEB:** https://core-electronics.com.au/
EMAIL: sapk0063@flinders.edu.au		**PHONE NO:** (02) 4027 5808	**EMAIL:** https://core-electronics.com.au/

QUANTITY	PART/CAT. NO.	DESCRIPTION	UNIT PRICE EX. GST	TOTAL COST EX. GST	ENTITY	COST CENTRE XXX	PROJECT XXXXX	EXPENSE CODE XXXX
6	CE04378	Adafruit NAU7802 24-Bit ADC - STEMMA QT / Qwiic	$ 11.52	$ 69.12	6			
1	BOB-16784	SparkFun Qwiic Mux Breakout - 8 Channel (TCA9548A)	$ 21.8	$ 21.8	1			
2	WRL-20168	SparkFun Thing Plus - ESP32 WROOM (USB-C)	$ 44.95	$ 89.9	2			
8	PRT-17260	Flexible Qwiic Cable - 50mm	$ 2.05	$ 16.4	8			
2	ADA4210	"JST SH 4-Pin Cable - Qwiic Compatible - 100mm LongSkip to the end of the images gallery"	$ 1.95	$ 3.9	2			
1	CAB-14743	USB 3.1 Cable A to C - 3 Foot	$ 10.5	$ 10.5	1			
7	CE04378	Polymer Lithium Ion Battery (LiPo) 3.7V 2000mAh	$	$ 0				
			TOTAL: $ 211.62					

Comment:

DO YOU REQUIRE QUOTES? *Please attach*		
VALUE	**QUOTATIONS REQUIRED**	
<$5,000	Single oral or written quote	☐
$5,000 to < $10,000	Two oral or written quotes	☐
$10,000 to < $15,000	Two written quotes	☐
$15,000 to < $100,000	Three written quotes	☐
> $100,000	Tender or RFP unless otherwise exempted	

PURCHASE AUTHORISATION

I authorise payment of this purchase(s) against the account(s) as detailed above, and acknowledge my responsibilities in ensuring that the purchase is being made in accordance with:

1) Flinders University Financial Services Policies and Procedures** http://www.flinders.edu.au/finance/

2) Flinders University Work Health and Safety Policies and Procedures for risk assessment* prior to the purchase of hazardous chemicals and plant http://www.flinders.edu.au/whs/

NAME:

Flinders UNIVERSITY
College of Science & Engineering

College Store

Requisition for Purchase

Date	Area	Ext No.	Buyer's Initials	Purchase Reference
10/08/2023	/ CSE	/	/	/

DELIVER TO: FLINDERS UNIVERSITY, SCIENCE & ENGINEERING STORE, PHYSICAL SCIENCES ROAD, BEDFORD PARK, SA 5042
EMAIL TO: cse.store@flinders.edu.au

REQUESTOR DETAILS			
NAME:	Deepak Sapkota		
ROOM NO:	Tonsley-3.22	**PHONE NO:**	0406566801
SUPERVISOR:	Dr. Amir Zanj		
EMAIL:	sapk0063@flinders.edu.au		

SUPPLIER DETAILS			
NAME:	RS Components Pty Ltd		
ADDRESS:	25 Pavesi St, Smithfield. NSW. 2164		
CONTACT:	1300 656 636	**WEB:**	https://au.rs-online.com/web/p/surface-mount-resistors/1978255
PHONE NO:	1300 656 636	**EMAIL:**	SupportAU@rs.rsgroup.com

QUANTITY	PART/CAT. NO.	DESCRIPTION	UNIT PRICE EX. GST	TOTAL COST EX. GST	ENTITY	COST CENTRE XXX	PROJECT XXXXX	EXPENSE CODE XXXX
1	Mfr. Part No.: AC12	Yageo 120Ω, 1206 (3216M) Thick Film Resistor ±1% 0.25W - AC1206FR-07120RL 100 units	$ 4.5	$ 4.5	01			
			TOTAL: $ 4.5					

Comment:

DO YOU REQUIRE QUOTES? *Please attach*		
VALUE	**QUOTATIONS REQUIRED**	
<$5,000	Single oral or written quote	☐
$5,000 to < $10,000	Two oral or written quotes	☐
$10,000 to < $15,000	Two written quotes	☐
$15,000 to < $100,000	Three written quotes	☐
> $100,000	Tender or RFP unless otherwise exempted	

PURCHASE AUTHORISATION

I authorise payment of this purchase(s) against the account(s) as detailed above, and acknowledge my responsibilities in ensuring that the purchase is being made in accordance with:

1) Flinders University Financial Services Policies and Procedures** http://www.flinders.edu.au/finance/

2) Flinders University Work Health and Safety Policies and Procedures for risk assessment* prior to the purchase of hazardous chemicals and plant http://www.flinders.edu.au/whs/

NAME: Amir Zanj

SIGN: Amir Zanj Digitally signed by Amir Zanj Date: 2023.08.11 10:33:48 +09'30'

Figure 25: list of procurements

APPENDIX H: Specification of the 3D printings

Table 10: Specifications of 3D printings

Parameters	**Specifications**
Fineness	0.1mm fine
Infill density	35%
Support Parameters	Touching the buildplate with a 40° overhang angle.
Estimated Weight	90g

Figure 26: 3D printed Central Blade

APPENDIX I: DEVELOPMENT OF TEST MODEL

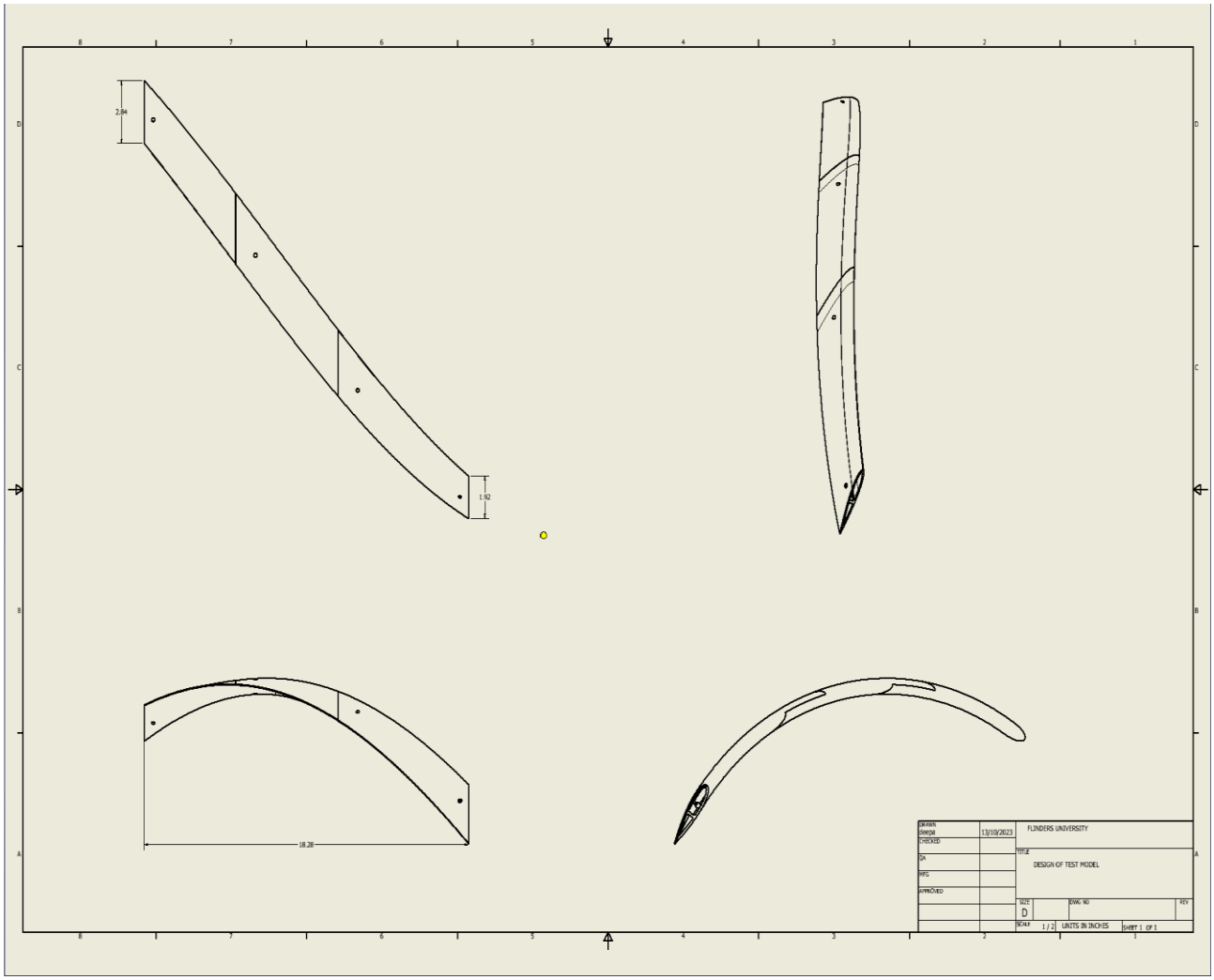

Figure 27: CAD Drawings of the Whole Test Model

Appendix J: CAD Drawings of Each sectionized blade of the test model.

1. Left side blade profile (towards the direction of strain gage)

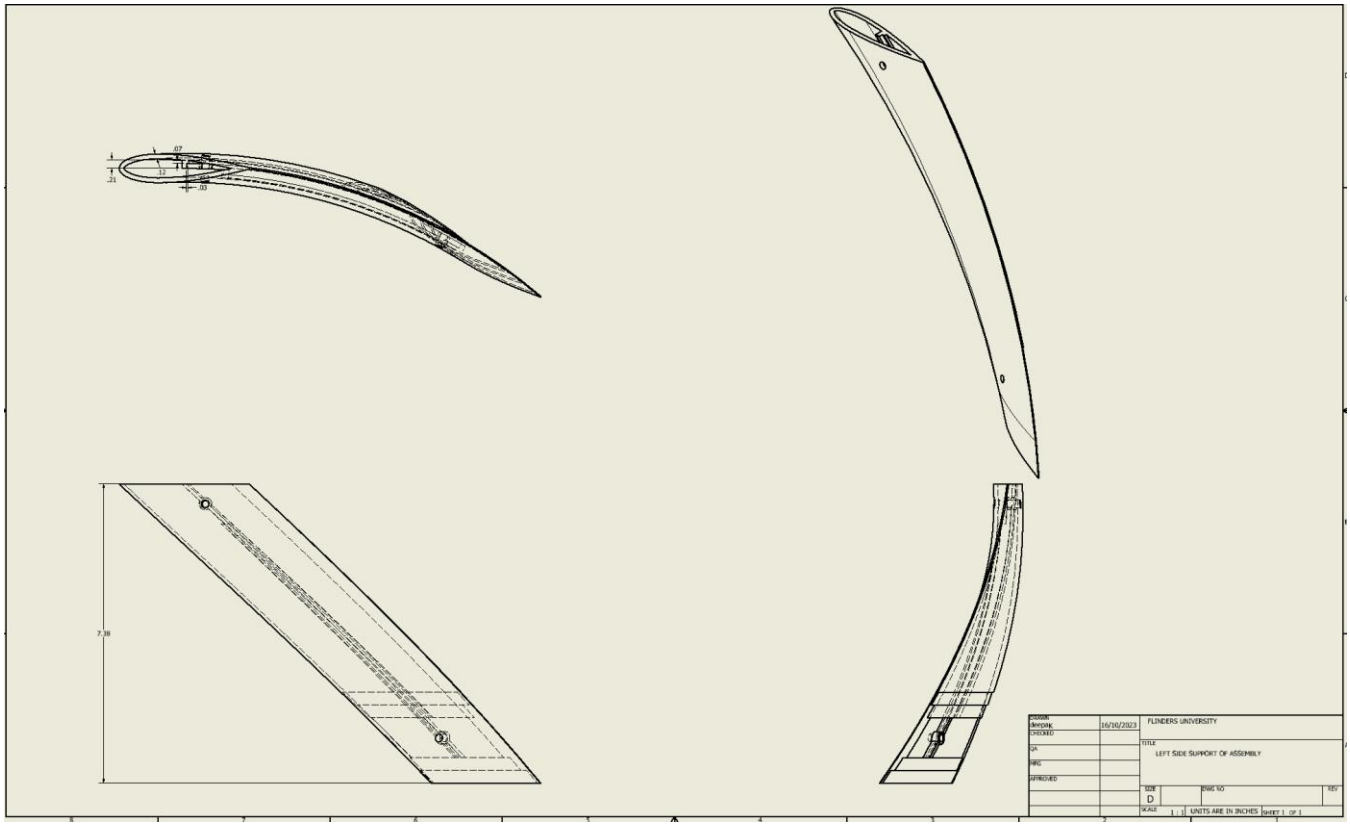

Figure 28: CAD drawing of Left side blade profile (towards the direction of Strain gage)

2. Right Side Blade (against the direction of strain gage)

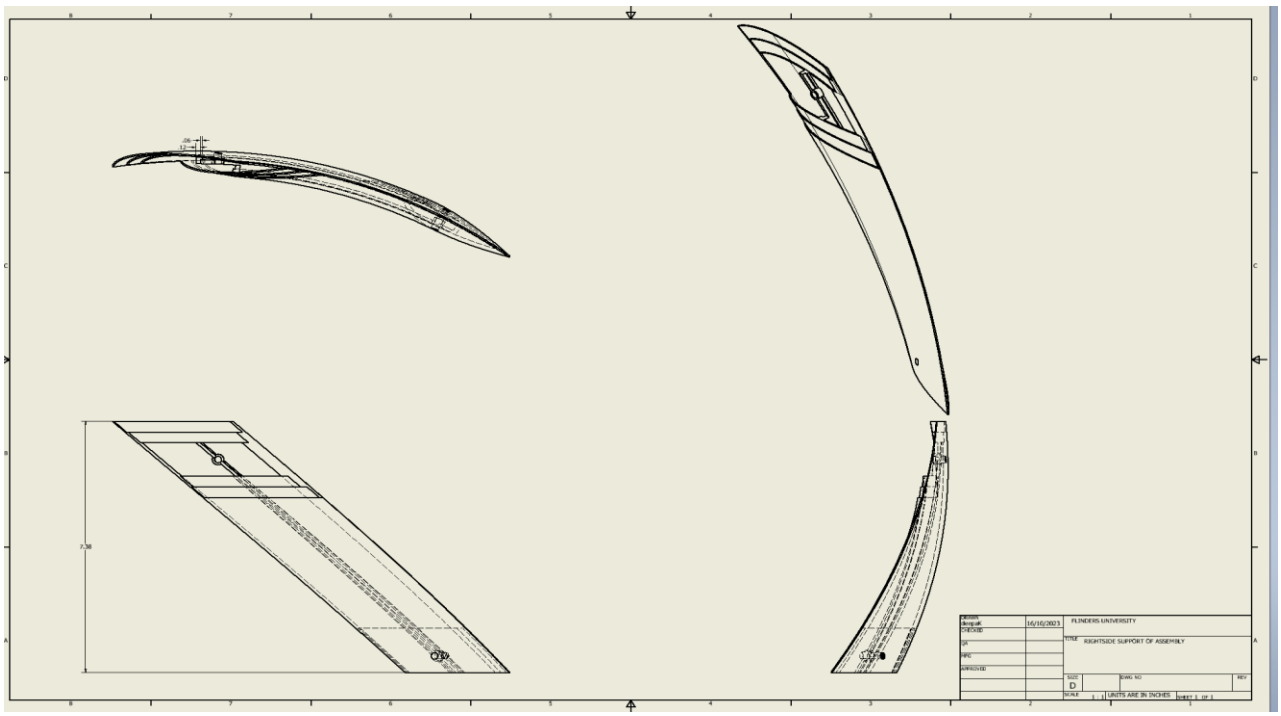

Figure 29: CAD drawing of Right Side blade (against the direction of strain gage)

3. Central Blade

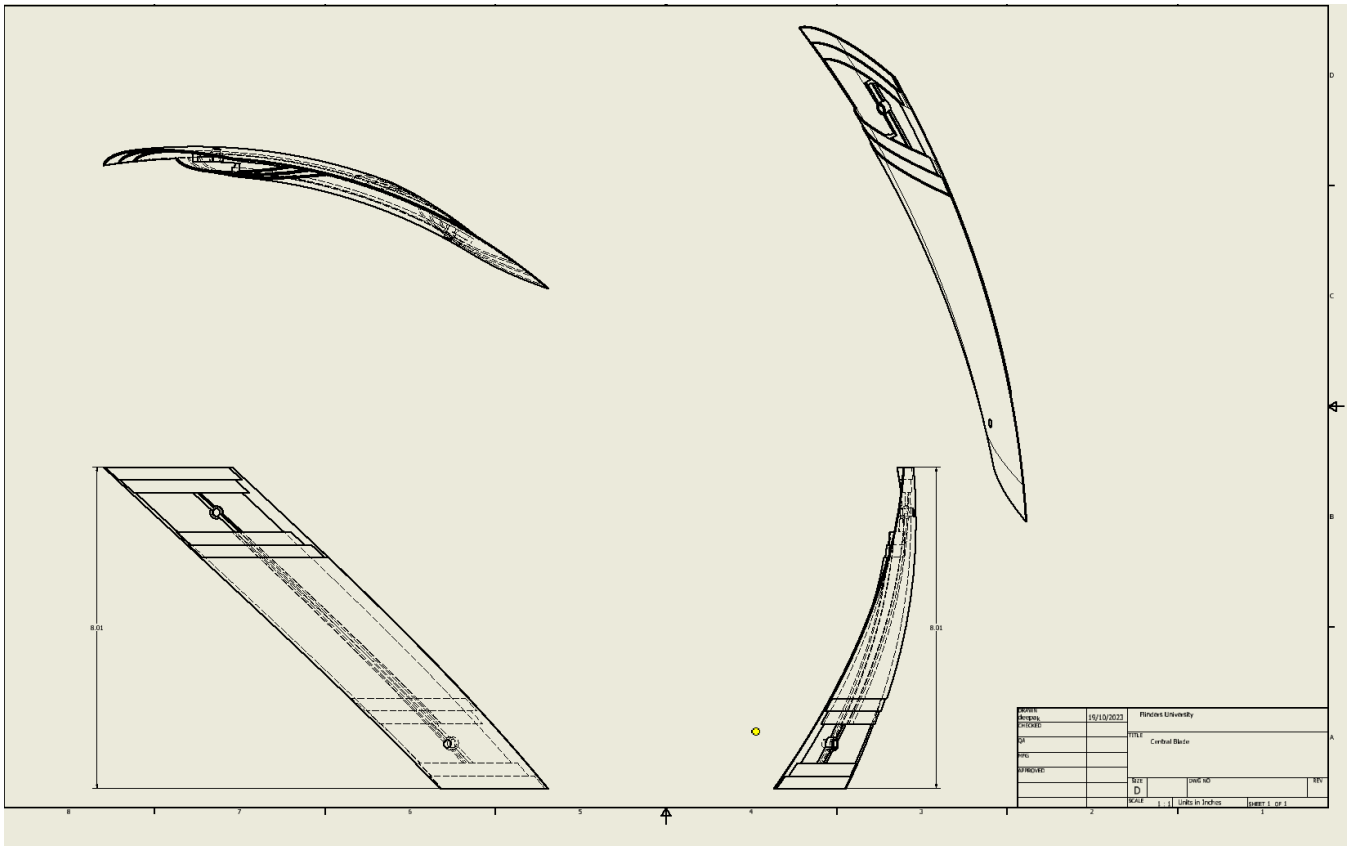

Figure 30: CAD Drawings of Central Blade

APPENDIX K: Arduino Programming Code for Experimentation

```
#include <Wire.h>

#include <SparkFun_I2C_Mux_Arduino_Library.h>  //Click here to get the library:
http://librarymanager/All#SparkFun_I2C_Mux
QWIICMUX myMux;



#include <Adafruit_NAU7802.h>  //Click here to get the library:
http://librarymanager/All#SparkFun_VL53L1X

Adafruit_NAU7802 **strain sensor;  //Create pointer to a set of pointers to the sensor
class
#define NUMBER_OF_SENSORS 3
void setup() {
  Serial.begin(115200);
  Serial.println("Qwiic Mux Shield Read Example");

  Wire.begin();

  //Create set of pointers to the class
  strainSensor = new Adafruit_NAU7802 *[NUMBER_OF_SENSORS];

  //Assign pointers to instances of the class
  for (int x = 0; x < NUMBER_OF_SENSORS; x++)
    strainSensor[x] = new Adafruit_NAU7802;

  if (myMux.begin() == false) {
    Serial.println("Mux not detected. Freezing...");
    while (1)
      ;
  }
  Serial.println("Mux detected");

  byte currentPortNumber = myMux.getPort();
  Serial.print("CurrentPort: ");
  Serial.println(currentPortNumber);

  //Initialize all the sensors
  bool initSuccess = true;

  for (byte x = 0; x < NUMBER_OF_SENSORS; x++) {
    myMux.setPort(x);
    if (!strainSensor[x]->begin())  //Begin returns 0 on a good init
    {
```

```
      Serial.print("Sensor ");
      Serial.print(x);
      Serial.println(" did not begin! Check wiring");
      initSuccess = false;
    } else {
      //Configure each sensor
      strainSensor[x]->setLDO(NAU7802_3V0);
      strainSensor[x]->setGain(NAU7802_GAIN_64);
      strainSensor[x]->setRate(NAU7802_RATE_10SPS);

      while (!strainSensor[x]->calibrate(NAU7802_CALMOD_INTERNAL)) {
        Serial.println("Failed to calibrate internal offset, retrying!");
        delay(1000);
      }
      Serial.println("Calibrated internal offset");

      while (!strainSensor[x]->calibrate(NAU7802_CALMOD_OFFSET)) {
        Serial.println("Failed to calibrate system offset, retrying!");
        delay(1000);
      }
      Serial.println("Calibrated system offset");
    }
  }

  if (initSuccess == false) {
    Serial.print("Freezing...");
    while (1)
      ;
  }

  Serial.println("Mux Shield online");
}

void loop() {
  int strain[NUMBER_OF_SENSORS];
  float strainFeet;

  for (byte x = 0; x < NUMBER_OF_SENSORS; x++) {
    myMux.setPort(x);  //Tell mux to connect to this port, and this port only
    while (!strainSensor[x]->available()) {
      delay(1);
    }
    int32_t val = strainSensor[x]->read();

    /*Serial.print("Reading ");
    Serial.print(x);
    Serial.print(": ");*/
    Serial.print(val);
    Serial.print(",");

  }
```

```
  Serial.println();

  delay(180);  //Wait for next reading
```

APPENDIX L: Experimentation

Figure 31: Experimentation Setup

APPENDIX M: CAD Designs

1. Assembly of ESP32 with its base

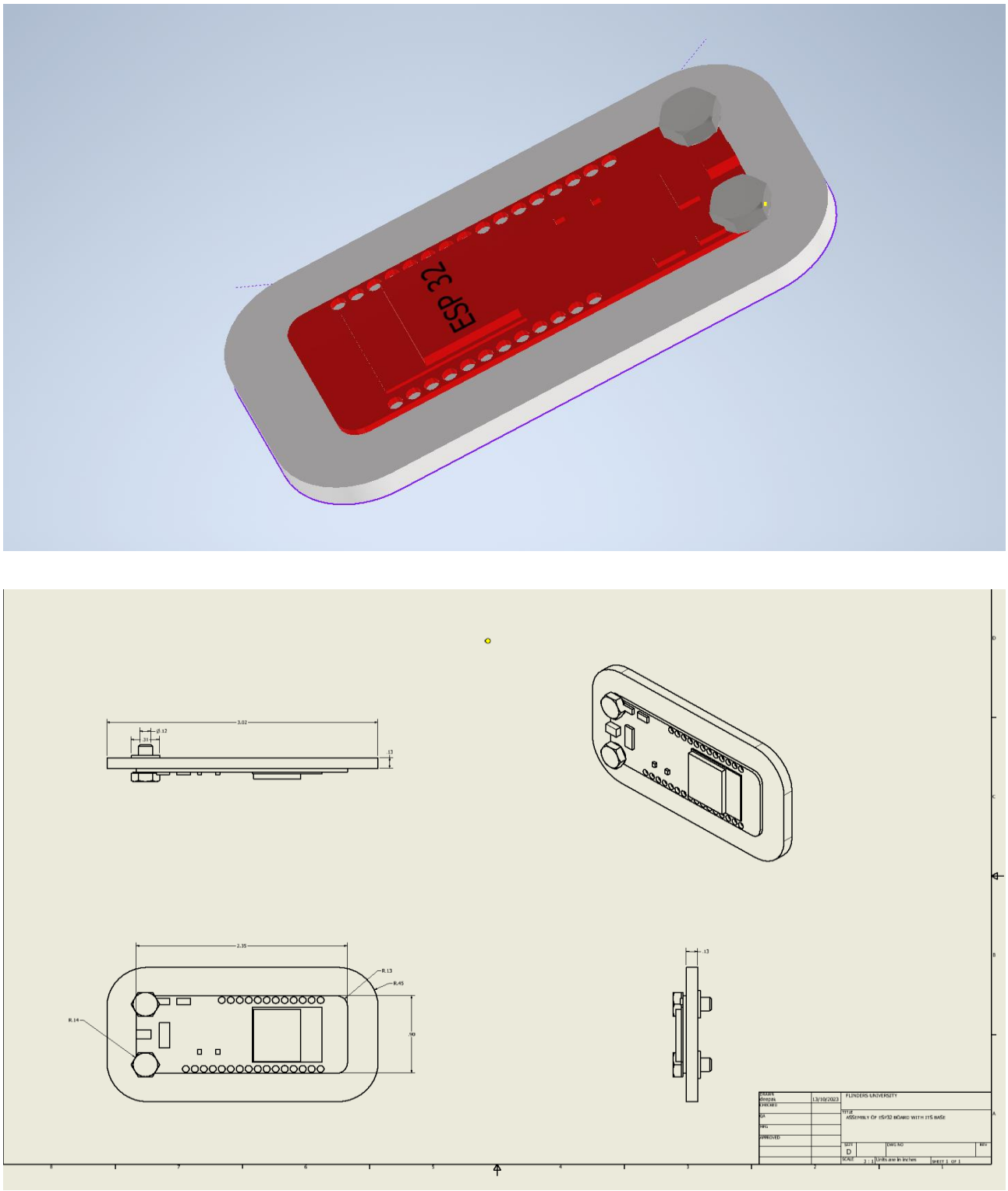

Figure 32: Design of ESP32 model with its base

2. Assembly of MUX board with its base

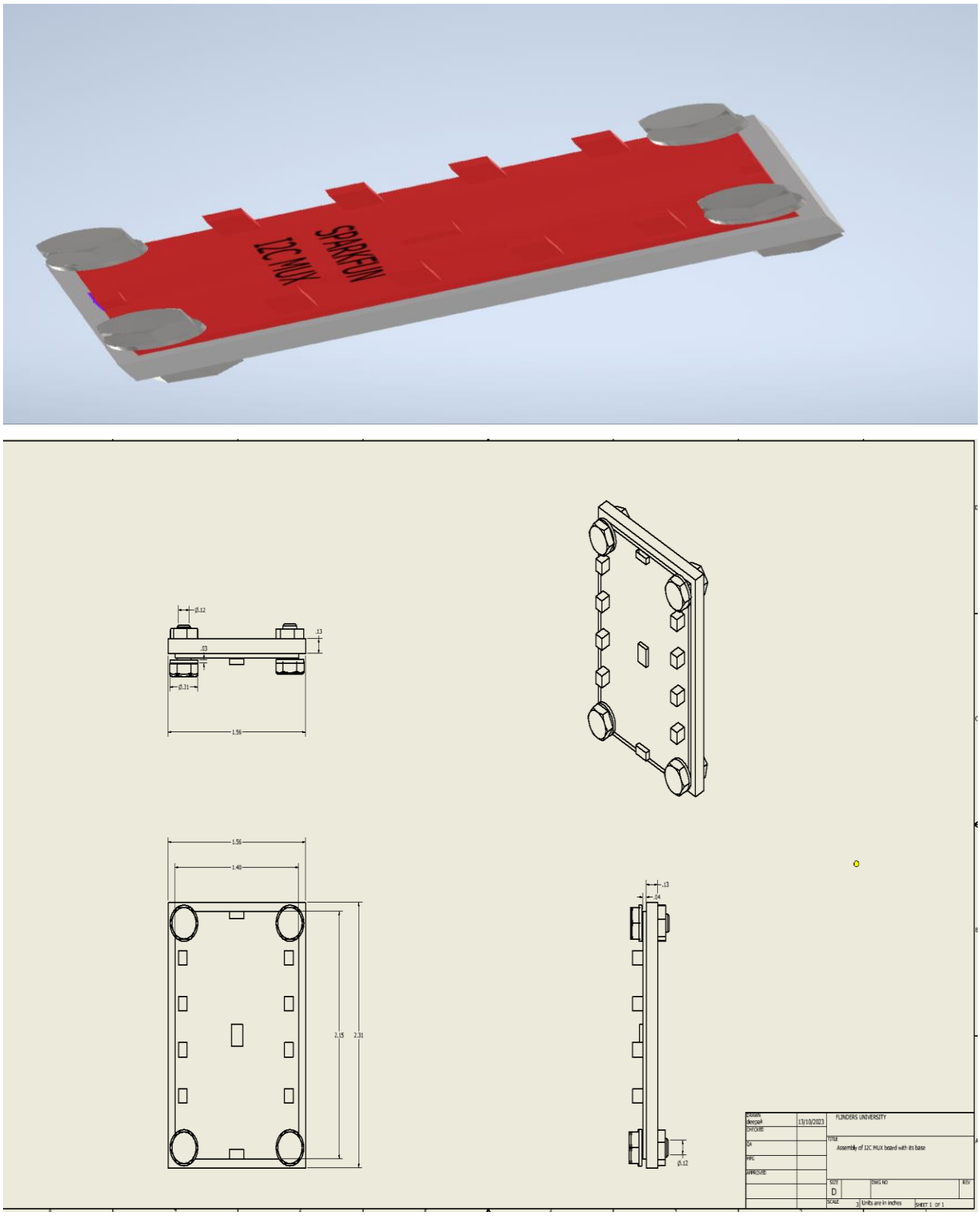

Figure 33: Design of MUX board with its base

3. Assembly of New Hollow Blades with Electronics Holder

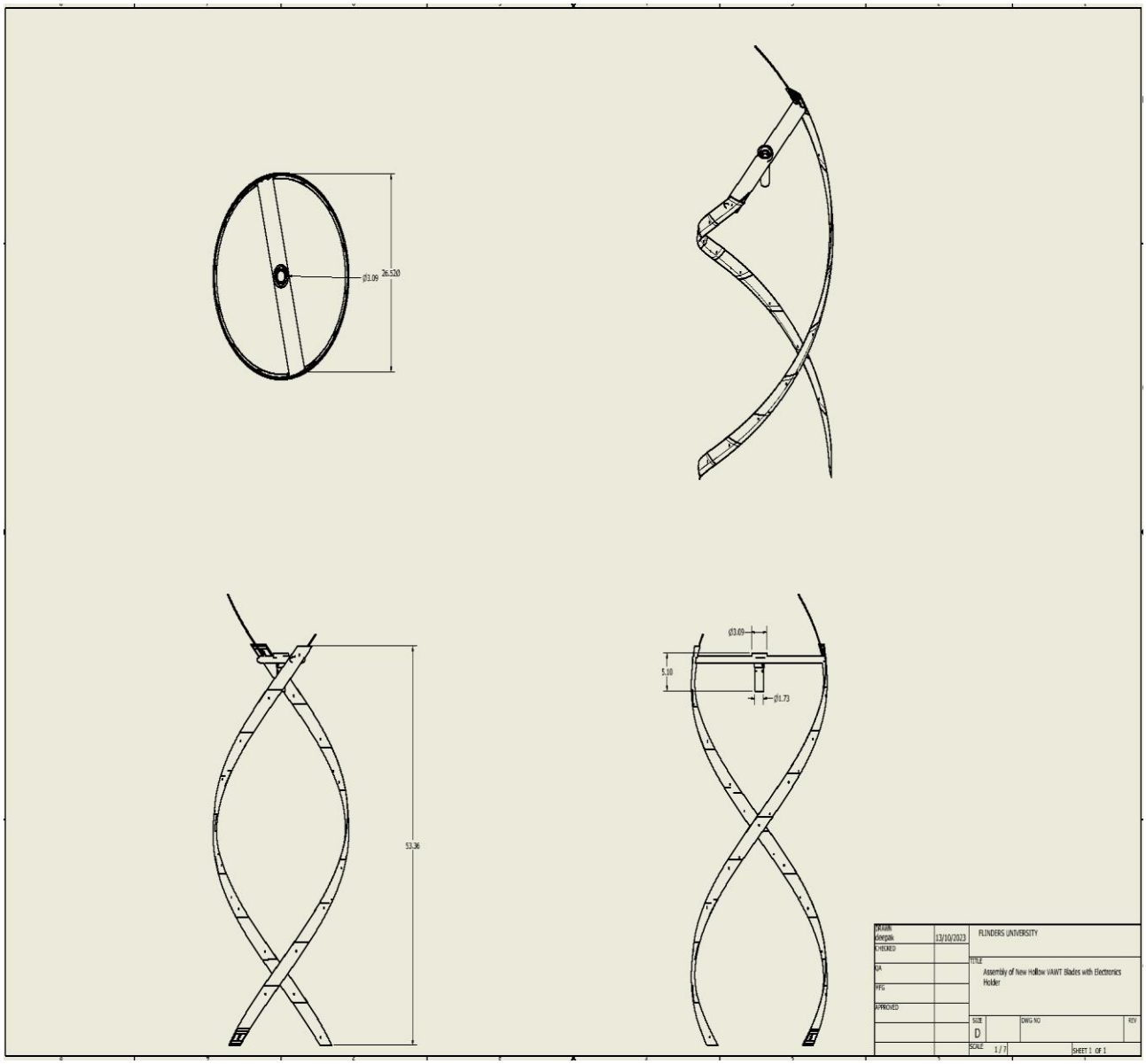

Figure 34: CAD Design of Assembly of New Blade Model

4. Design of Electronics Holder

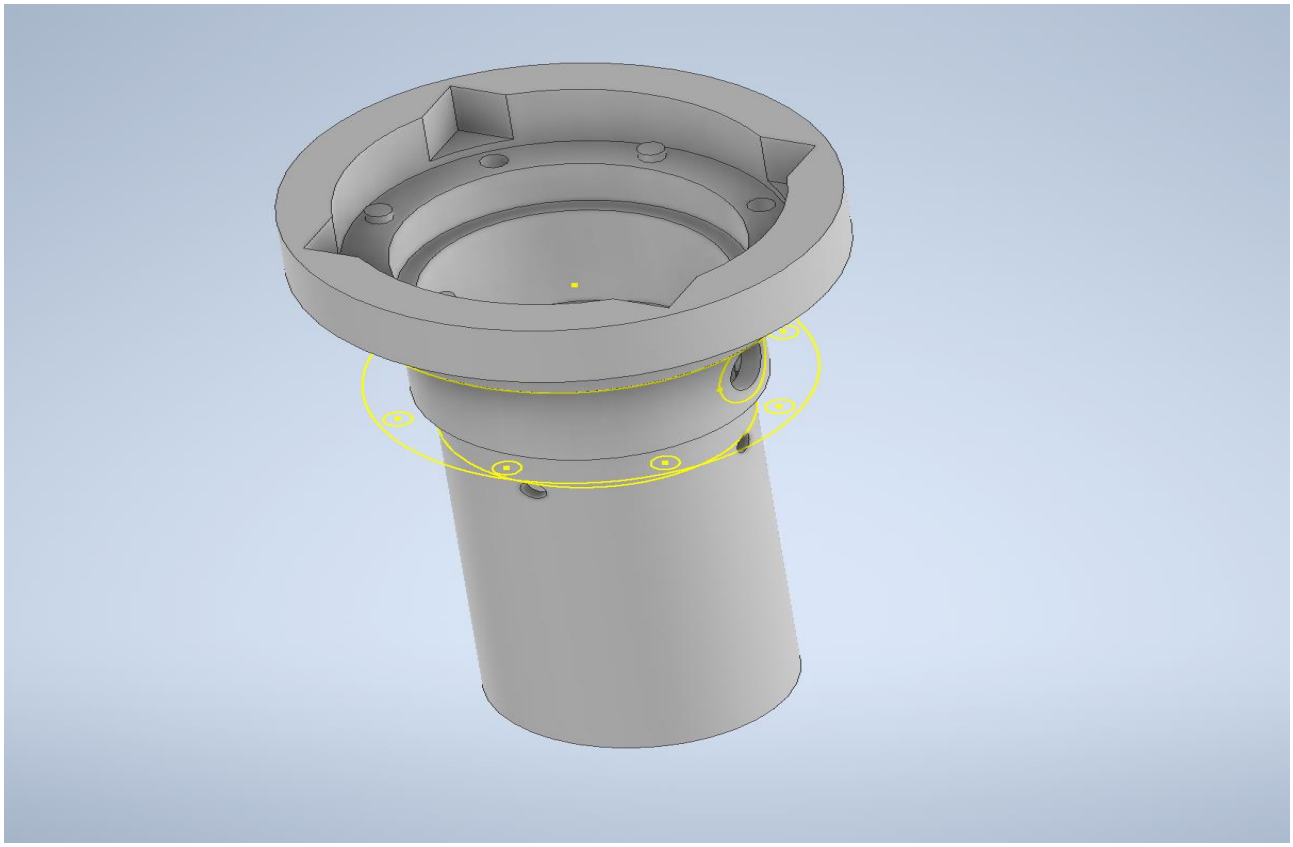

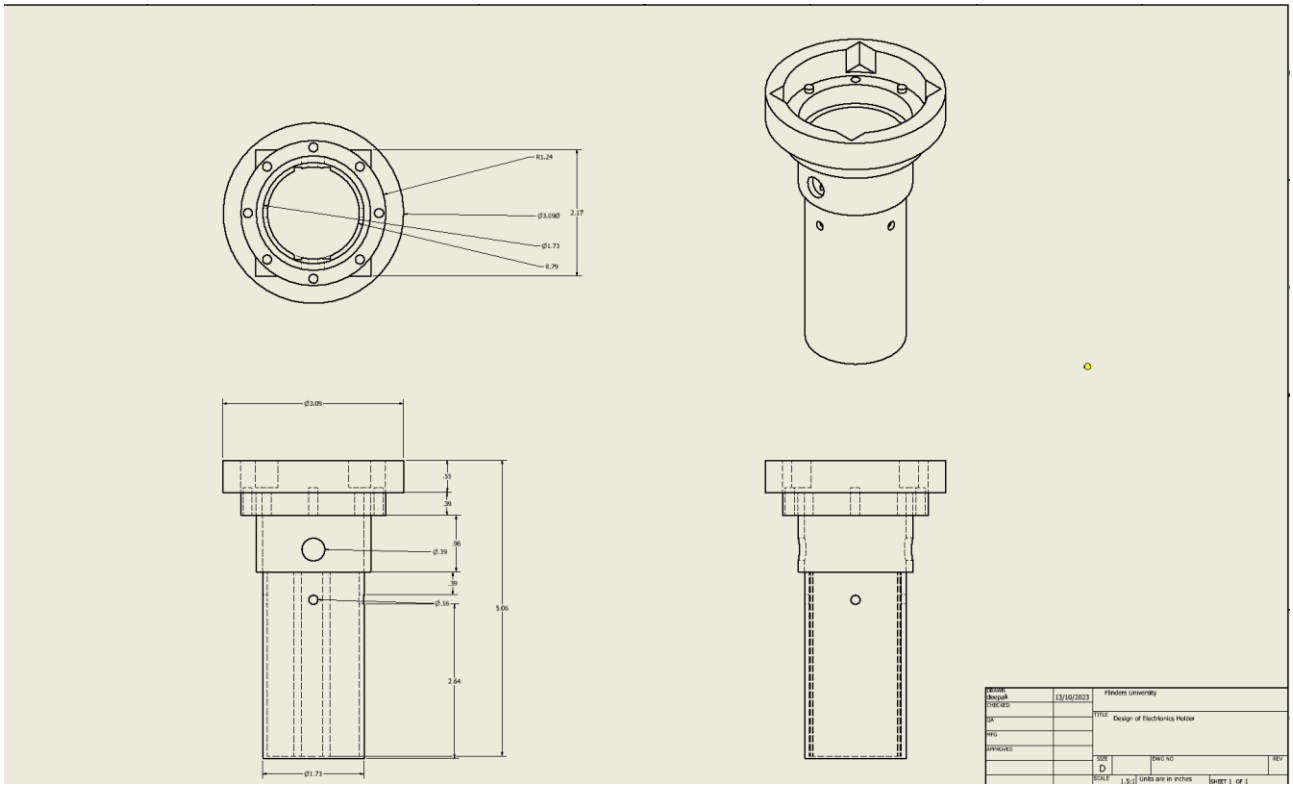

Figure 35: Designs of Electronics Holder

Appendix N: Experimental Calculations

$Voltage\ value = \frac{\Delta Digital\ values}{2^n - 1} * \frac{V_{ref}}{Gain}$ From eqn (1) from methodology; (SparkFun, n.d.)

For voltage-to-strain conversion; $V_0 = \frac{VEX}{4} * K * \epsilon$

i.e., $\epsilon = \frac{4}{VEX * k} * V0$

1. For 3.5 N Loadings

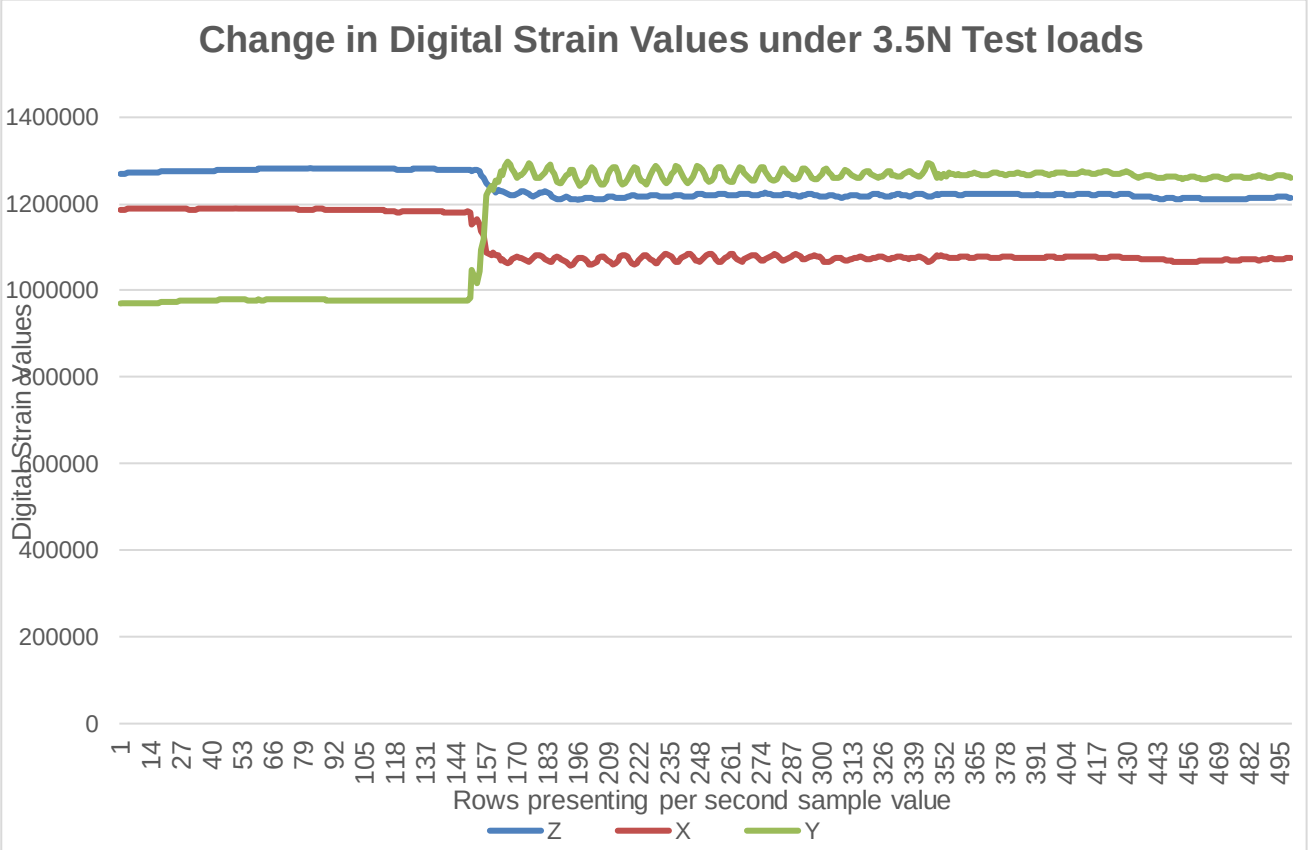

Figure 36: Change of Digital Strain values along the experimentation for 3.5N loadings at each end

For 3.5N loads

Table 11: Calculation of Voltages and Strains for 3.5N loadings at each end

Strain Gage	Average Digital value before loading	Average digital value after loading	Change in the digital value	Generated Differential Voltage Output	Strain-induced
Strain Gage (X-axis)	1182694	1077316	105378	0.2355mV	152.427μ∈ i.e. (ϵ_1)

Strain Gage (Y-axis)	978652	1271295	292643	0.6541mV	423.365 μ∈ (ϵ_2)
Strain Gage (Z-axis)	1280903	1222592	58311	0.130mV	84.142 μ∈ i.e.(ϵ_3)

Table 12: Calculations of Strains and stresses for 3.5N loadings on each end

Parameters	**Formula**	**Calculated Value**
Maximum Principal Strain (ϵ_{max})	$\frac{1}{2}[\epsilon_1+\epsilon_2+\sqrt{2*\{(\epsilon_1-\epsilon_3)^2+(\epsilon_2-\epsilon_3)^2\}}$	**532.574 μ∈**
Minimum Principal Strain (ϵ_{min})	$\frac{1}{2}[\epsilon_1+\epsilon_2-\sqrt{2*\{(\epsilon_1-\epsilon_3)^2+(\epsilon_2-\epsilon_3)^2\}}$	**43.217μ∈**
Maximum Shearing Strain (γ_{max})	$\sqrt{2*\{(\epsilon_1-\epsilon_3)^2+(\epsilon_2-\epsilon_3)^2\}}$	**489.356μ∈**
Maximum Principal Stress (σ_{max})	$\frac{E}{1-\nu^2}(\epsilon_{max}+\nu\,\epsilon_{min})$	**1.460MPa**
Minimum Principal Stress (σ_{min})	$\frac{E}{1-\nu^2}(\epsilon_{min}+\nu\,\epsilon_{max})$	**0.612MPa**
Maximum Shearing Stress (ζ_{max})	$\frac{E}{2(1+\nu)}\gamma_{max}$	**0.424MPa**
Stress Intensity	$\frac{E}{(1+\nu)}\gamma_{max}$	**0.848MPa**

2. For 17N loadings

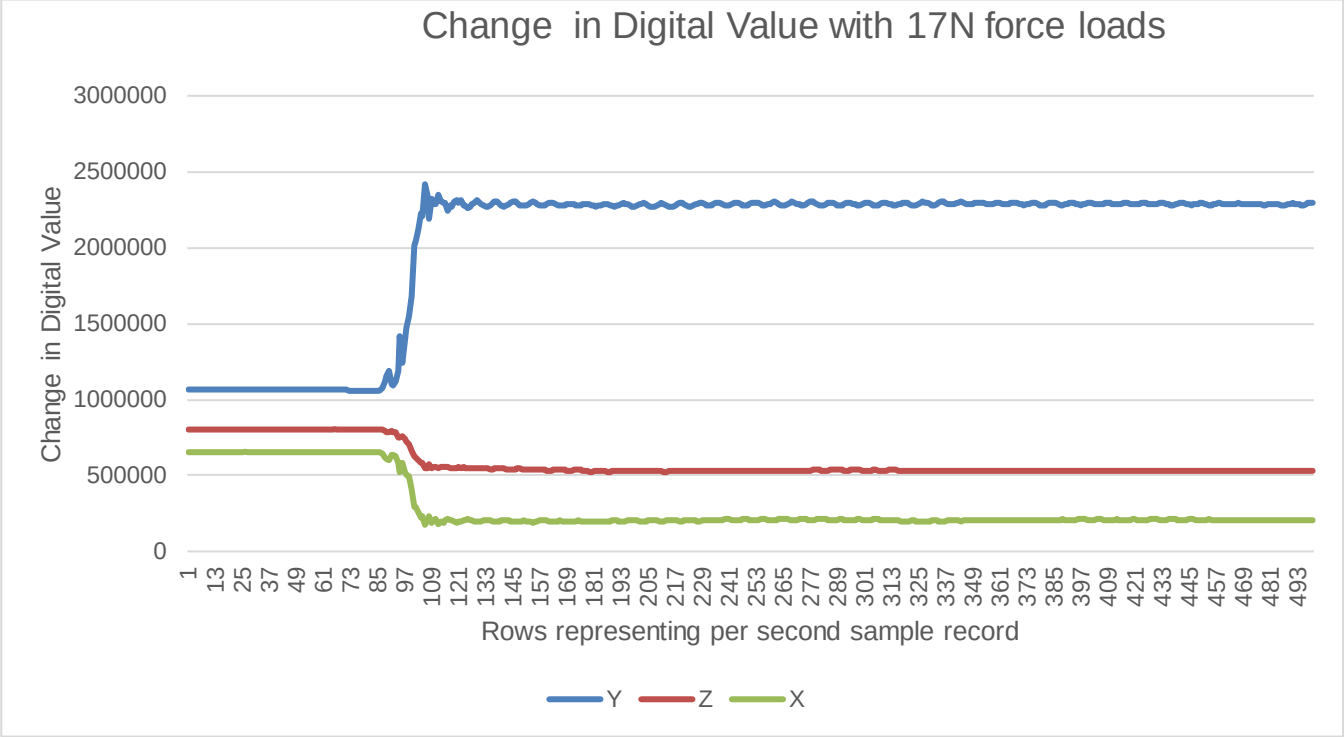

Figure 37: Change of Digital Strain values along the experimentation for 17N loadings at each end

Table 13: Calculation of Voltages and Strains for 17N loadings at each end

Strain Gage	Average Digital value before loading	Average digital value after loading	Change in the digital value	Generated Differential Voltage Output	Strain-induced
Strain Gage (X-axis)	655910	201683	454227	1.01mV	653.721 μϵ (ϵ_1)
Strain Gage (Y-axis)	1064239	2298794	1234555	2.759mV	1785.76 μϵ i.e. (ϵ_2)
Strain Gage (Z-axis)	805187	530826	274361	0.613mV	396.763 μϵ i.e. (ϵ_3)

Table 14: Calculations of Strains and stresses for 17N loadings on each end

Parameters	**Formula**	**Calculated Value**
Maximum Principal Strain($\in_{max}$)	$\frac{1}{2}\left[\in_1+\in_2+\sqrt{2*\{(\in_1-\in_3)^2+(\in_2-\in_3)^2\}}\right.$	**2218.574μ∈**
Minimum Principal Strain($\in_{\min}$)	$\frac{1}{2}\left[\in_1+\in_2-\sqrt{2*\{(\in_1-\in_3)^2+(\in_2-\in_3)^2\}}\right.$	**220.9061 μ∈**
Maximum Shearing Strain (γ_{max})	$\sqrt{2*\{(\in_1-\in_3)^2+(\in_2-\in_3)^2\}}$	**1997.668 μ∈**
Maximum Principal Stress (σ_{max})	$\frac{E}{1-\nu^2}\left(\in_{max}+\nu\in_{min}\right)$	**6.12MPa**
Minimum Principal Stress (σ_{min})	$\frac{E}{1-\nu^2}\left(\in_{min}+\nu\in_{max}\right)$	**2.659MPa**
Maximum Shearing Stress (ζ_{max})	$\frac{E}{2(1+\nu)}\gamma_{max}$	**1.731MPa**
Stress Intensity	$\frac{E}{(1+\nu)}\gamma_{max}$	**3.462MPa**

3. For 12N loadings

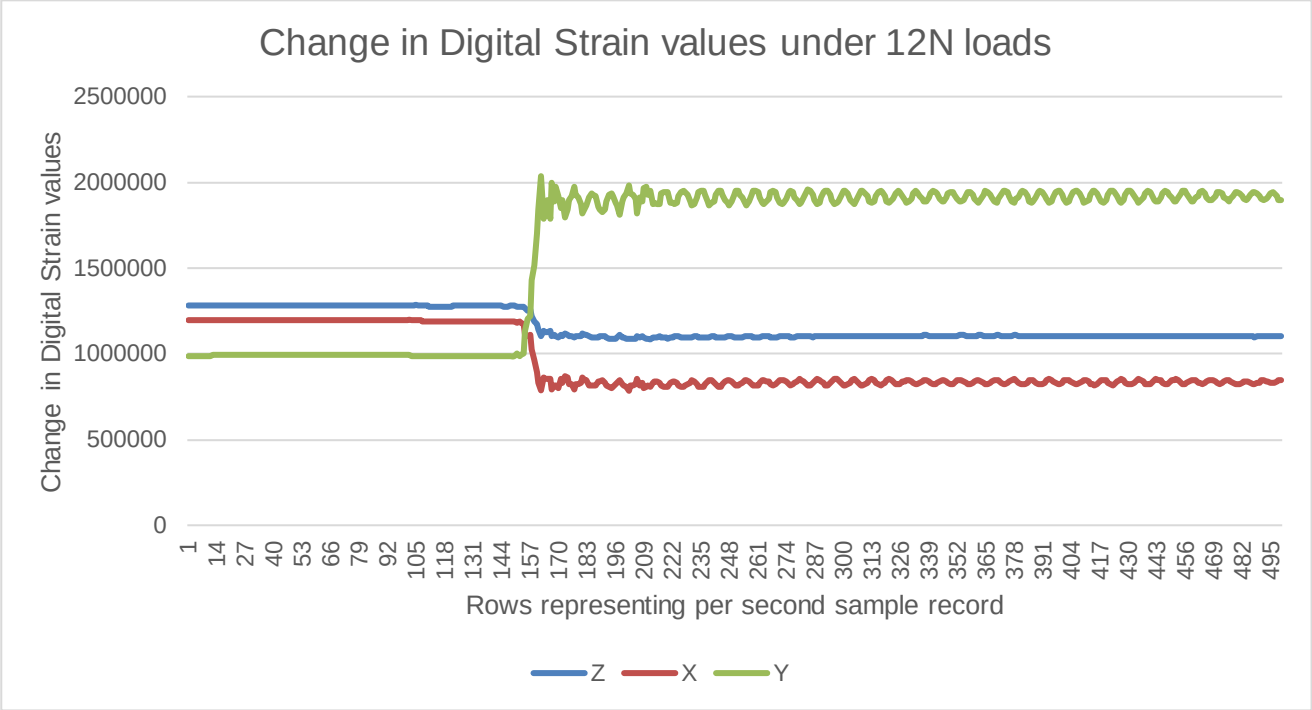

Figure 38: Change of Digital Strain values along the experimentation for 12N loadings at each end.

Table 15: Calculation of Voltages and Strains for 12N loadings at each end

Strain Gage	Average Digital value before loading	Average digital value after loading	Change in the digital value	Generated Differential Voltage Output	Strain-induced
Strain Gage (X-axis)	1191129	823352	367777	0.822mV	532.038 μϵ i.e. (ϵ_1)
Strain Gage (Y-axis)	986386	1951617	965231	2.1574mV	1396.375μϵ (ϵ_2)
Strain Gage (Z-axis)	1279218	1099315	179903	0.402mV	260.194 ϵ i.e.(ϵ_3)

Table 16:Calculations of Strains & Stresses for 12 N loadings on each end

Parameters	**Formula**	**Calculated Value**
Maximum Principal Strain(ϵ_{max})	$\frac{1}{2}\left[\epsilon_1+\epsilon_2+\sqrt{2*\{(\epsilon_1-\epsilon_3)^2+(\epsilon_2-\epsilon_3)^2\}}\right.$	**1790.283μ∈**
Minimum Principal Strain(ϵ_{min})	$\frac{1}{2}\left[\epsilon_1+\epsilon_2-\sqrt{2*\{(\epsilon_1-\epsilon_3)^2+(\epsilon_2-\epsilon_3)^2\}}\right.$	**138.129μ∈**
Maximum Shearing Strain (γ_{max})	$\sqrt{2*\{(\epsilon_1-\epsilon_3)^2+(\epsilon_2-\epsilon_3)^2\}}$	**1652.154 μ∈**
Maximum Principal Stress (σ_{max})	$\frac{E}{1-\nu^2}\left(\epsilon_{max}+\nu\,\epsilon_{min}\right)$	**4.903MPa**
Minimum Principal Stress (σ_{min})	$\frac{E}{1-\nu^2}\left(\epsilon_{min}+\nu\,\epsilon_{max}\right)$	**2.039Pa**
Maximum Shearing Stress (ζ_{max})	$\frac{E}{2(1+\nu)}\gamma_{max}$	**1.431MPa**
Stress Intensity	$\frac{E}{(1+\nu)}\gamma_{max}$	**2.862MPa**

4. For 10.5N loadings

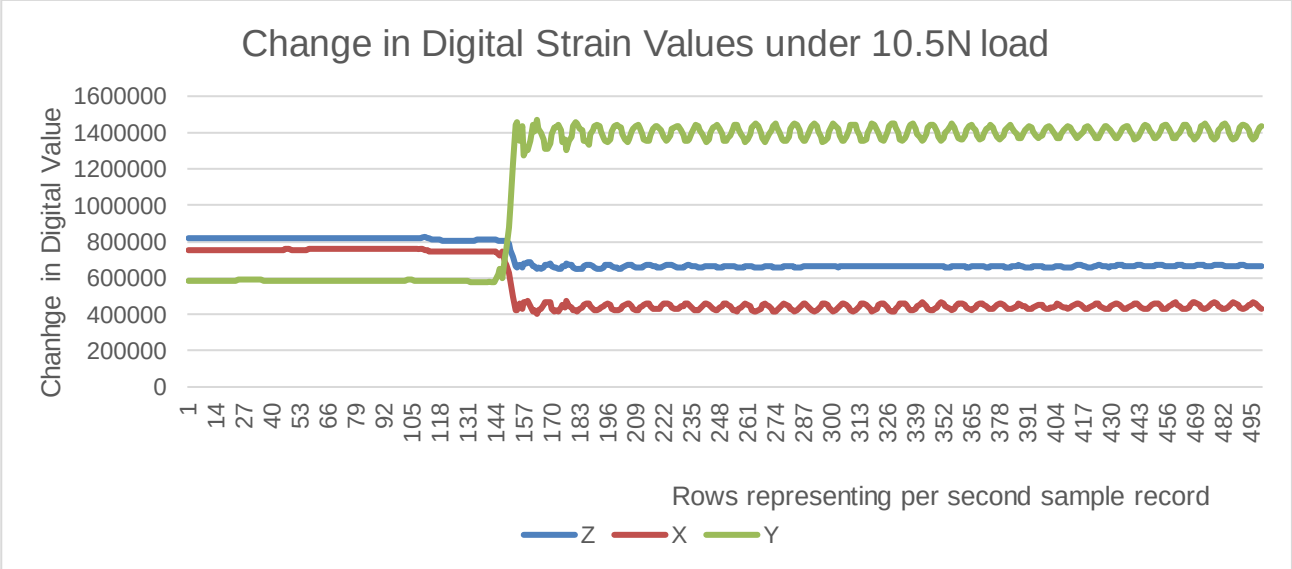

Figure 39: Change of Digital Strain values along the experimentation for 10.5N loadings at each end.

Table 17: Calculation of Voltages and Strains for 10.5N loadings at each end

Strain Gage	Average Digital value before loading	Average digital value after loading	Change in the digital value	Generated Differential Voltage Output	Strain-induced
Strain Gage (X-axis)	742603	415017	327586	0.7322mV	473.786μ ∈ i.e. (ϵ_1)
Strain Gage (Y-axis)	581460	1106270	524810	1.17mV	757.281 μ∈ μ∈ (ϵ_2)
Strain Gage (Z-axis)	805569	659754	145815	0.325mV	210.035μ ∈ i.e.(ϵ_3)

Table 18: Calculations of Strains and stresses for 10.5N loadings on each end

Parameters	**Formula**	**Calculated Value**
Maximum Principal Strain(ϵ_{max})	$\frac{1}{2}\,[\epsilon_1+\epsilon_2+\sqrt{2*\{(\epsilon_1-\epsilon_3)^2+(\epsilon_2-\epsilon_3)^2\}}$	**1606.360μ∈**
Minimum Principal Strain($\epsilon_{\min}$)	$\frac{1}{2}\,[\epsilon_1+\epsilon_2-\sqrt{2*\{(\epsilon_1-\epsilon_3)^2+(\epsilon_2-\epsilon_3)^2\}}$	**105.734μ∈**
Maximum Shearing Strain (γ_{max})	$\sqrt{2*\{(\epsilon_1-\epsilon_3)^2+(\epsilon_2-\epsilon_3)^2\}}$	**1500.626μ∈**
Maximum Principal Stress (σ_{max})	$\frac{E}{1-\nu^2}\,(\,\epsilon_{max}+\nu\,\epsilon_{min})$	**4.38MPa**
Minimum Principal Stress (σ_{min})	$\frac{E}{1-\nu^2}\,(\,\epsilon_{min}+\nu\,\epsilon_{max})$	**1.781MPa**

Maximum Shearing Stress (ζ_{max})	$\frac{E}{2(1+\nu)}\gamma_{max}$	**1.30MPa**
Stress Intensity	$\frac{E}{(1+\nu)}\gamma_{max}$	**2.60MPa**

Appendix O: FEA Analysis

A: Loading conditions

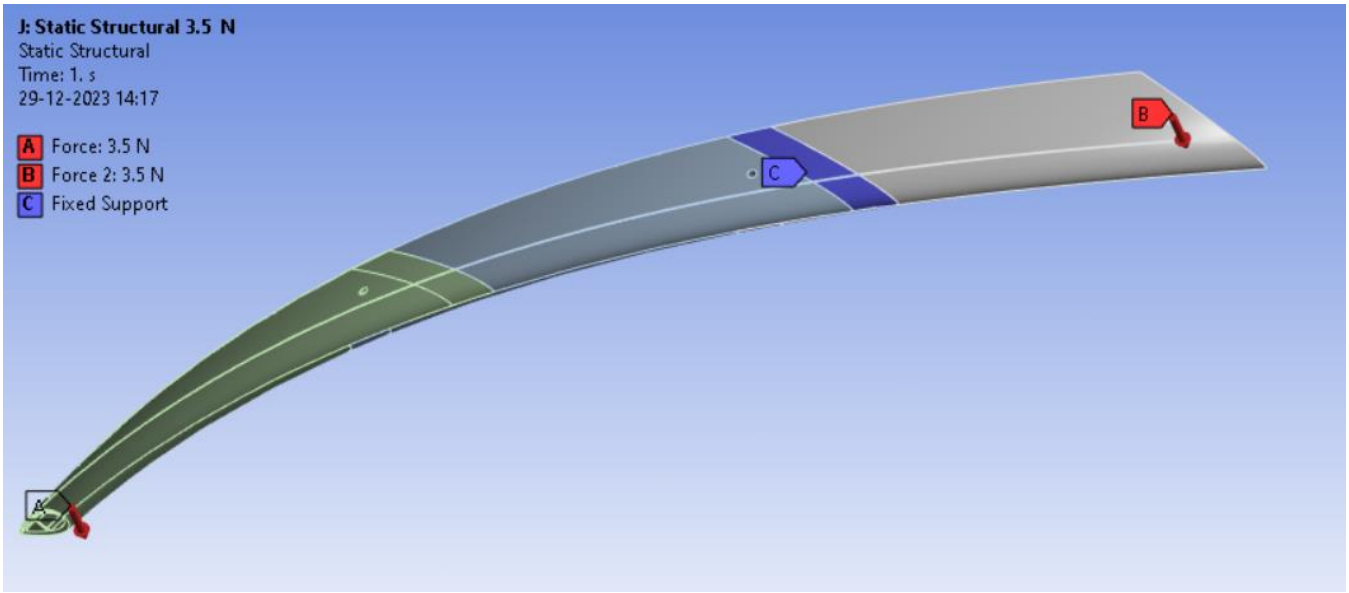

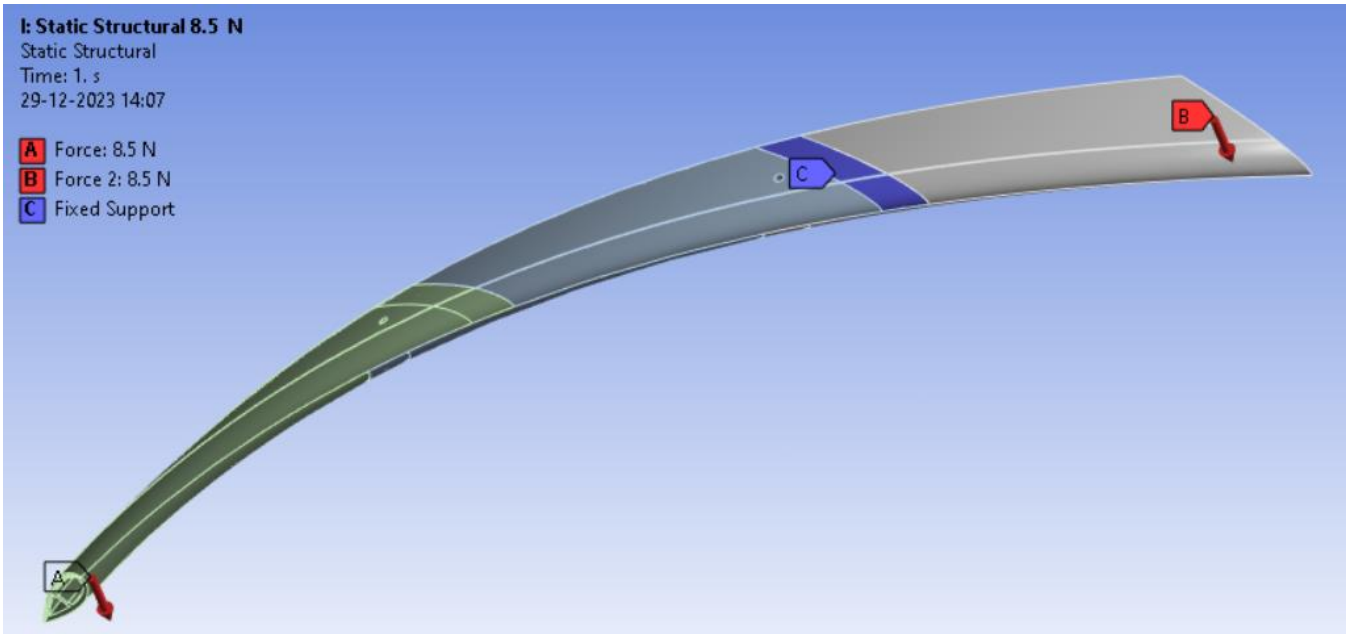

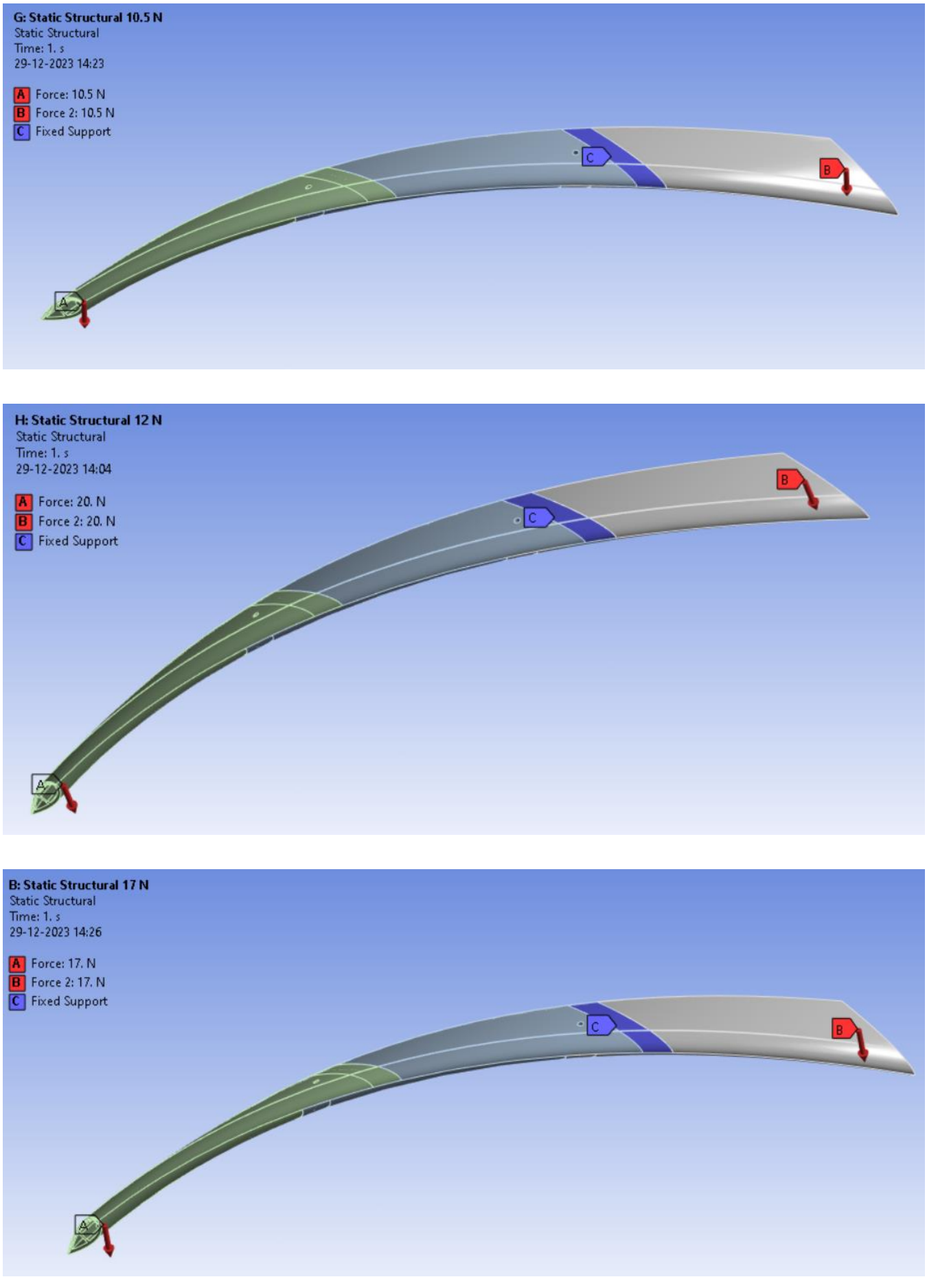

Figure 40: Loading Conditions for various loading conditions

B: FEA Results:

i). 3.5N

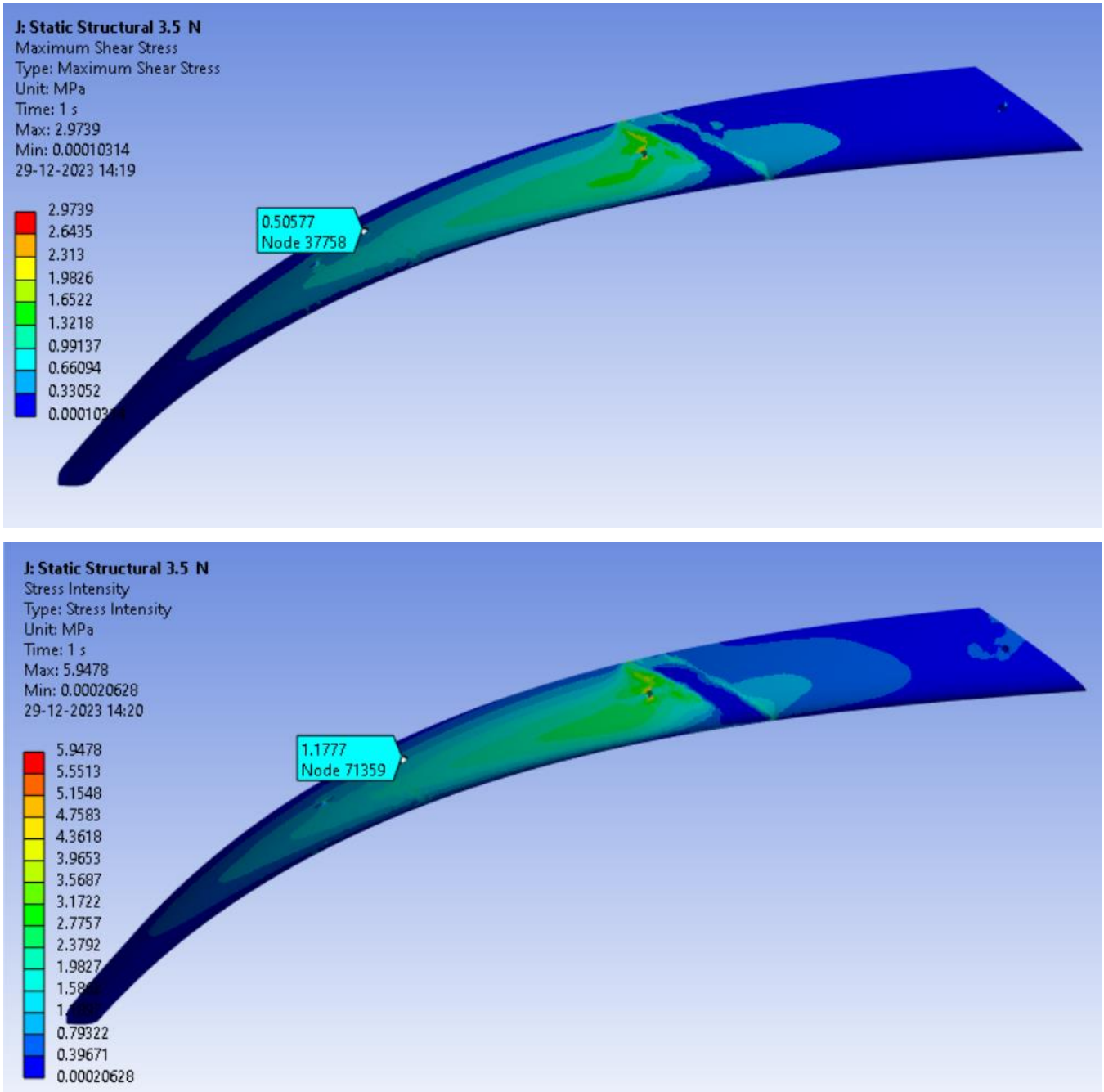

Figure 41: FEA Analysis for 3.5N loadings at each end

ii). 8.5 N

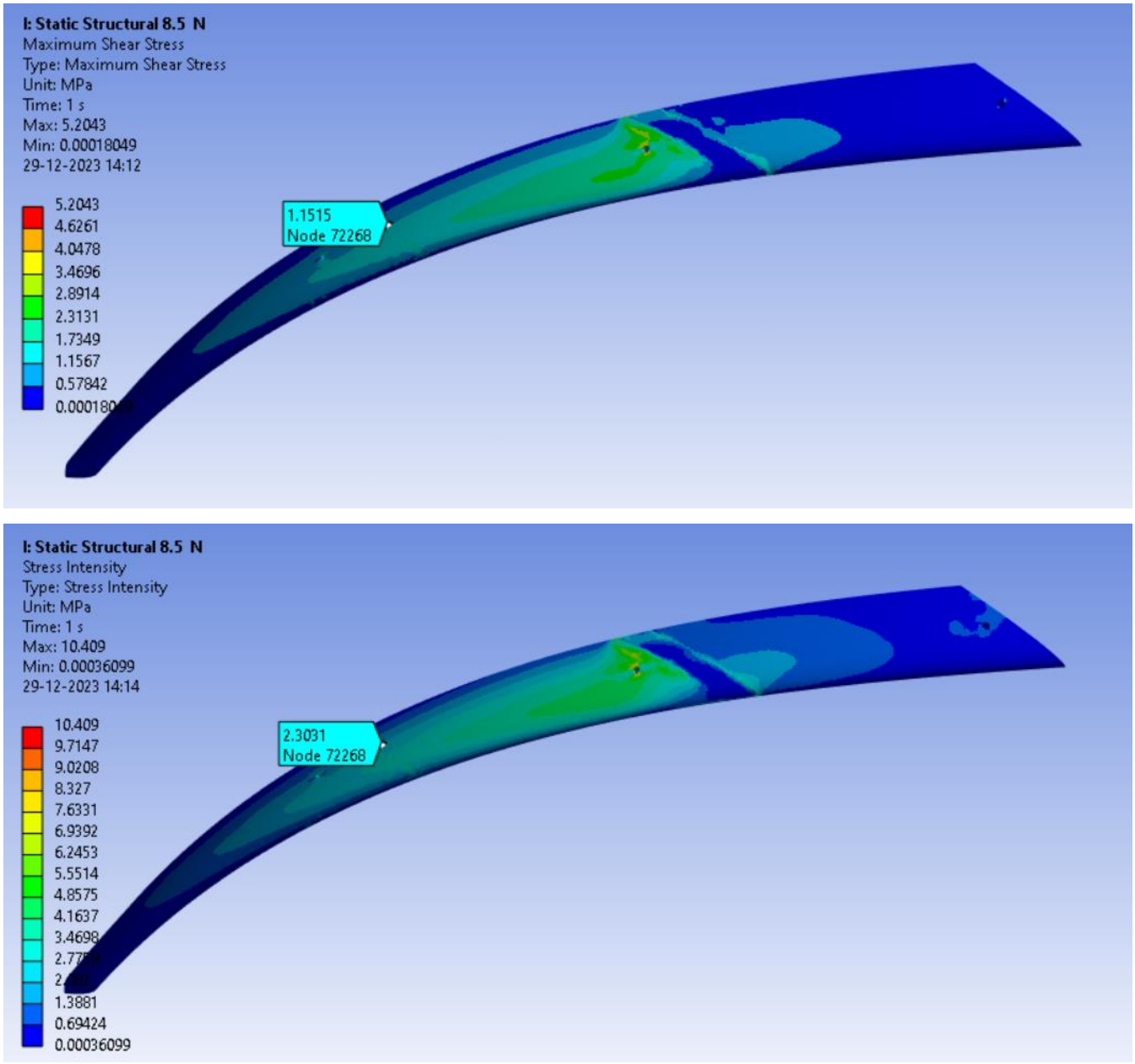

Figure 42: FEA Analysis of 8.5N loadings at each end

iii). 10.5 N

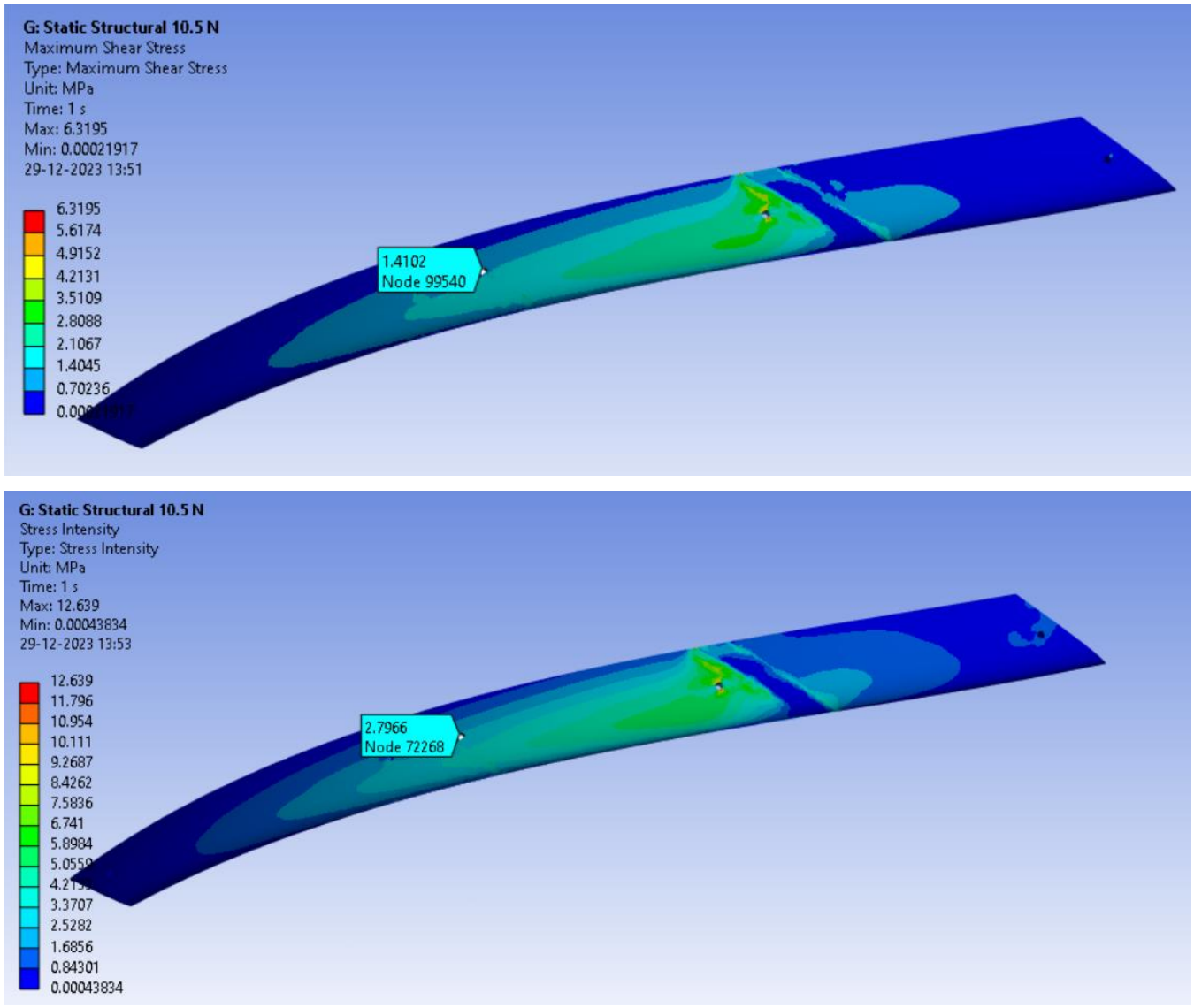

Figure 43: FEA Analysis of 10.5N for each end

iv). 12 N

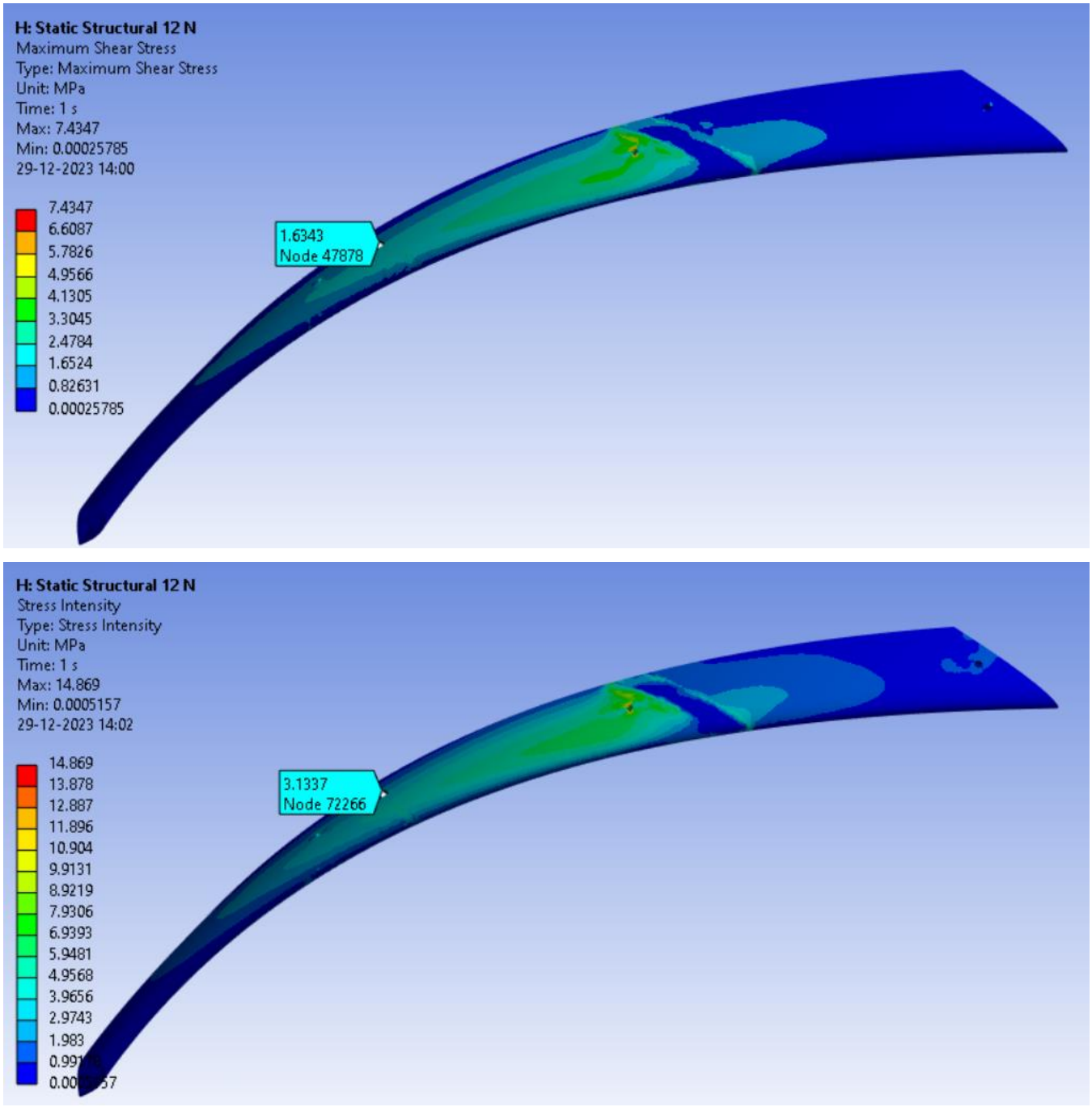

Figure 44: FEA Analysis of 12N loadings for each end.

v. 17N

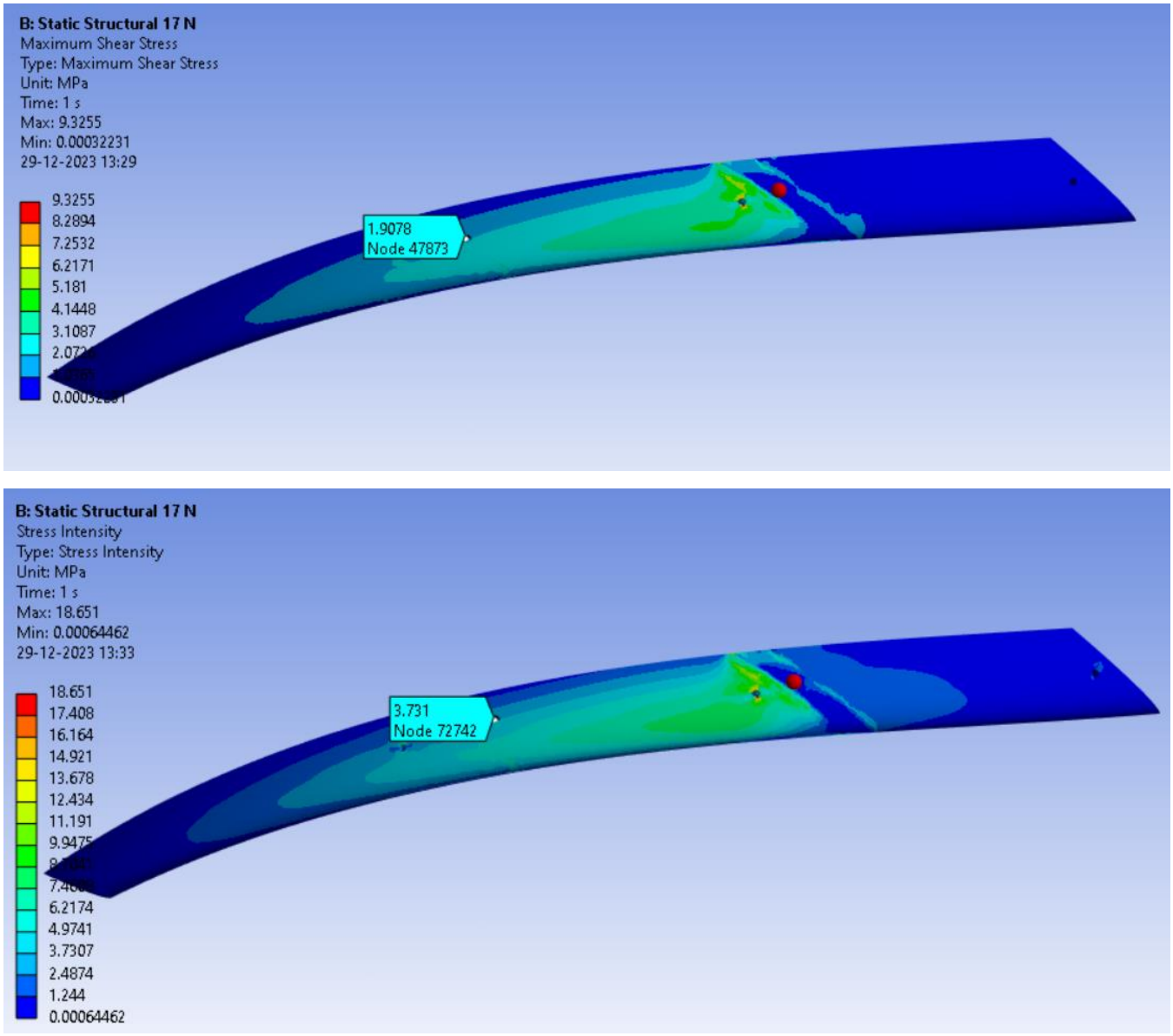

Figure 45: FEA Analysis of 17N loadings for each end.